UNIVERSITÀ DEGLI STUDI DI TRIESTE

XXXI CICLO DEL DOTTORATO DI RICERCA IN NANOTECNOLOGIE

DEVELOPMENT AND CHARACTERIZATION OF A POLYSACCHARIDE-BASE BIOMATERIAL FOR BIOMEDICAL APPLICATIONS

Settore scientifico-disciplinare: **BIO/10 - BIOCHIMICA**

DOTTORANDA
Federica Vecchies

COORDINATORE
Prof. Lucia Pasquato

SUPERVISORE DI TESI
Prof. Sergio Paoletti

CO-SUPERVISORI
Dr. Eleonora Marsich
Dr. Gianluca Turco

ANNO ACCADEMICO 2017/2018

UNIVERSITÀ DEGLI STUDI DI TRIESTE

XXXI CICLO DEL DOTTORATO DI RICERCA IN NANOTECNOLOGIE

DEVELOPMENT AND CHARACTERIZATION OF A POLYSACCHARIDES-BASE BIOMATERIAL FOR BIOMEDICAL APPLICATIONS

Settore scientifico-disciplinare: **BIO/10 - BIOCHIMICA**

DOTTORANDA
Federica Vecchies

COORDINATORE
Prof. Lucia Pasquato

SUPERVISORE DI TESI
Prof. Sergio Paoletti

CO-SUPERVISORI
Dr. Eleonora Marsich
Dr. Gianluca Turco

ANNO ACCADEMICO 2017/2018

For my family that gave me the possibility to achieve this goal.

For Gabri, who loves me, everyday.

It was a long road that brought me here to these days. Not all the days have been good, sometimes it was difficult, hard, and without a clear vision of what could be of my work. But I think that it is part of what is called "growing up". You don't see the whole picture until you finally got there. And that's what a PhD is. You start with the passion of a newly graduated master student, and down the road you find yourself in moments of trouble, pure joy or doubts. You learn how to listen, and how to get away on your own. You work a lot, sometimes too much. But that's part of the job.

But all these emotions worth nothing without someone to share them with. Thanks Pasquale, Michi, Fra and Franco for these amazing 3 years of works together, lunches together, laughter together.

Thanks to Gian and Davide for being like a family to me, always there when I needed.

Thanks to Andrea, Massi and Ivan for the advises and the help they gave me during this period.

Thanks to Eleonora, for guiding me and being such an inspiration in these 3 years.

Thanks to Professor Sergio Paoletti, my supervisor, because without him this path would not have begun.

PREFACE

This thesis is submitted in fulfillment to the requirements of the Graduate School of Nanotechnology for the academic title of Ph.D. in Nanotechnology at the University of Trieste. The work has been carried out mainly at the Department of Life Sciences at the University of Trieste under the supervision of Prof. Sergio Paoletti and co-supervised by Dr. Eleonora Marsich, Dr. Gianluca Turco. Part of the activity was performed at Biomaterial Lab of the Dental Clinic of Maggiore Hospital.

This study was supported by the INTERREG V-A ITALIA- SLOVENIA 2014-2020 BANDO 1/2016 ASSE 1 - project BioApp 1472551605. I also acknowledge the support by the ERA-MarineBiotech project Mar3Bio.

The thesis consists of a general introduction, aim of the study and a detailed discussion of results divided into three chapters.

SUMMARY

The repair of articular cartilage represents a huge challenge in the biomedical field. Articular cartilage is a thin layer between bone at the joint site, and despite its dimension, plays a key role in the distribution of the loads through the bones, and allows free movements of the joint, avoiding friction. Articular cartilage lacks of innervations, lymphatic stream and blood stream, and the chondrocytes (the main cell type) presented a poor proliferation ability. These conditions determine a serious problem when the tissue is damaged or affected by a disease. Unfortunately, articular cartilage is subjected to numerous trauma that can occur during life from long term wear, to physical injuries, but also inflammatory and genetic diseases. As a result, a progressive and irreversible degeneration of the cartilage could lead to changes also in the adjacent synovial and bone tissue resulting in an arthritis disease. Nowadays researchers are trying to overcome the more classical therapies (pharmacological treatment, viscosupplementation, arthroscopy, and autologus chondrocytes implantation), that are not able to completely restore the native tissue, by tissue engineering approaches.

The aim of the present work is to develop a biomaterial that could fit in the cartilage defect. Such biomaterial should possesses mechanical properties resemble that of the native tissue, intrinsic bioactivity to guide the repair, and a long-lasting sustained release of a therapeutic molecule.

In Chapter I, the miscibility studies of two oppositely charged polysaccharides , namely hyaluronic acid and CTL (lactose modified chitosan) were described. Investigations on the influence of several parameters that could affect the behavior of the two polymers were conducted. The possibility to prepared complex coacervates via electrostatic interaction between the two polyelectrolites was explored by Transmittance and Dynamic Light Scattering analyses.

The characterization of the coacervates is reported in Chapter II. Here, the possibility to stabilize the system in physiological conditions was investigated. The stability in physiological ionic strength, temperature and pH was achieved by using an EDC/NHS chemistry. The possibility to freeze-dry and store the coacervates for commercial purposes were also investigated. The loading efficacy and release kinetic of this system was accessed using a model payload. Lastly, the biocompatibility of the coacervates is reported and analysed.

The development of a bioactive hydrogel is described in Chapter III. Alginate, CTL and chondroitin sulfate were employed for hydrogel preparation. The gelification occurred by exploiting the ion diffusion technique. After the mechanical characterization of the structure, the integration of coacervates within the hydrogel was successfully explored.

Further *in vitro* and *in vivo* experiment should be conducted to complete the characterization of the whole system, but the data collected in this thesis proposed a promising biomaterials that may be considered for the treatment of articular cartilage defects.

SOMMARIO

La riparazione della cartilagine articolare rappresenta una grande sfida in campo biomedico. La cartilagine articolare è uno strato sottile che si trova tra due ossa a livello delle giunzioni articolari. Nonostante il suo spessore, svolge un ruolo chiave nella distribuzione dei carichi e permette alle ossa articolari di muoversi evitando l'attrito. La cartilagine articolare non presenta innervazione, e non è raggiunta da vasi linfatici o sanguigni. Inoltre, le cellule che compongono la cartilagine, i condrociti, presentano una scarsa capacità proliferativa. Tali condizioni determinano una scarsa capacità rigenerativa del tessuto. Sfortunatamente, la cartilagine articolare è soggetta a numerosi traumi che possono verificarsi durante la vita per usura a lungo termine, lesioni fisiche, o malattie infiammatorie e genetiche. Conseguentemente, una degenerazione progressiva e irreversibile della cartilagine potrebbe portare a cambiamenti anche nei tessuti sinoviale e osseo adiacenti, con conseguente sviluppo di patologie quali osteoartrite e malattie reumatiche.

Attualmente i ricercatori stanno cercando di superare le terapie più classiche (trattamento farmacologico, viscosupplamentazione, artroscopia e impianto di condrociti autologhi), che non sono in grado di ripristinare completamente il tessuto nativo, sfruttando l'approccio dell'ingegneria tissutale.

Lo scopo del presente lavoro è quello di sviluppare un biomateriale capace di riempire il difetto cartilagineo, dotato di proprietà meccaniche simili a quelle del tessuto nativo, di bioattività intrinseca per guidare la riparazione della cartilagine e capacità di garantire un rilascio prolungato di una molecola bioattiva (farmaco o fattore di crescita).

Nel Capitolo I sono stati descritti gli studi di miscibilità di due polisaccaridi con carica opposta, vale a dire acido ialuronico e CTL. E' stata esaminata l'influenza di pH, forza ionica, peso molecolare e rapporto quantitativo tra i due polimeri sul comportamento della soluzione binaria. La

possibilità di preparare coacervati tramite l'interazione elettrostatica tra i due polielettroliti è stata valutata mediante analisi di trasmittanza e dynamic light scattering.

La caratterizzazione dei coacervati è riportata nel Capitolo II. Qui è stata studiata la possibilità di stabilizzare il sistema in condizioni fisiologiche. La formazione dei coacervati avviene immediatamente dopo il gocciolamento dell'acido ialuronico nella soluzione di CTL. I coacervati si sono subito dimostrati stabili in condizioni di forza ionica e temperatura fisiologiche, mentre hanno mostrato una dissoluzione dipendente dal pH. La stabilità in funzione del pH è stata ottenuta utilizzando un cross-linker chimico. E' stata valutata anche la possibilità di liofilizzare e conservare i coacervati per scopi commerciali. L'efficienza di caricamento e la cinetica di rilascio di questo sistema è stata valutata utilizzando una molecola modello. Infine, viene presentata una valutazione della biocompatibilità dei coacervati.

Lo sviluppo di un idrogele bioattivo è descritto nel Capitolo III. Alginato, CTL e condroitin solfato sono stati impiegati per la preparazione dell'idrogele. La gelificazione avviene sfruttando la tecnica della diffusione ionica. Dopo la caratterizzazione meccanica della struttura, l'integrazione dei coacervati all'interno dell'idrogele è stata ottenuta con successo.

Ulteriori esperimenti *in vitro* e *in vivo* devono essere condotti per completare la caratterizzazione dell'intero sistema, ma i dati raccolti in questa tesi propongono un biomateriale che può essere preso in considerazione per il trattamento dei difetti della cartilagine articolare.

LIST OF PAPERS

Federica Vecchies, Pasquale Sacco, Eva Decleva, Renzo Menegazzi, Davide Porrelli, Ivan Donati, Gianluca Turco, Sergio Paoletti and Eleonora Marsich. "*Complex Coacervates between a Lactose-Modified Chitosan and Hyaluronic Acid as Radical-Scavenging Drug Carriers*". Biomacromolecules, 2018; 19, 3936−3944.

Gianluca Turco, Davide Porrelli, Eleonora Marsich, **Federica Vecchies**, Teresa Lombardi, Claudio Stacchi and Roberto Di Lenarda. "*Three-Dimensional Bone Substitutes for Oral and Maxillofacial Surgery: Biological and Structural Characterization*". Journal of Functional Biomaterials, 2018; 9(4), 62.

SYMBOLS AND ABBREVIATIONS

HA	Hyaluronic acid
CS	Chondroitin sulfate
CTL	Lactose modified chitosan
Alg	Alginate
ECM	Extracellular matrix
OA	Osteoarthritis
RA	Rheumatoid arthritis
ROS	Reactive oxygen species
DAMPs	Damage associated molecular patterns
NSAIDs	Nonsteroidal anti-inflammatory drugs
COX2	Cyclooxygenase 2
TE	Tissue engineering
MSCs	Mesenchymal stromal cells
MHC-II	Major histocompatibility complex of class II
PGA	Polyglycolic acid
PRP	Platelet rich plasma
COMP	Cartilage oligomeric matrix protein

PE	polyelectrolyte
TNF	Tumor necrosis factor
TPP	Tripolyphosphate
PPi	Pyrophosphate
MW	Molecular weight
F_A	Fraction of actetylated units
DP	Degree of polymerization
T	Transmittance
I	Ionic strength
DLS	Dynamic light scattering
PDI	Polydispersity index
FBG	Fibrinogen
DHR	Dihydrorhodamine
HRP	Horseradish peroxidase
TEM	Transmission electron microscopy

TABLE OF CONTENTS

1. INTRODUCTION

1.1 Articular Cartilage

Articular cartilage is a thin layer of hyaline cartilage that covers opposing articulating bones.[1] Despite the size of the tissue, ranging from 2 to 4 mm thick, articular cartilage has a primary importance allowing free movements between bones, distributing the loads and resisting to compressive, tensile and shear forces.

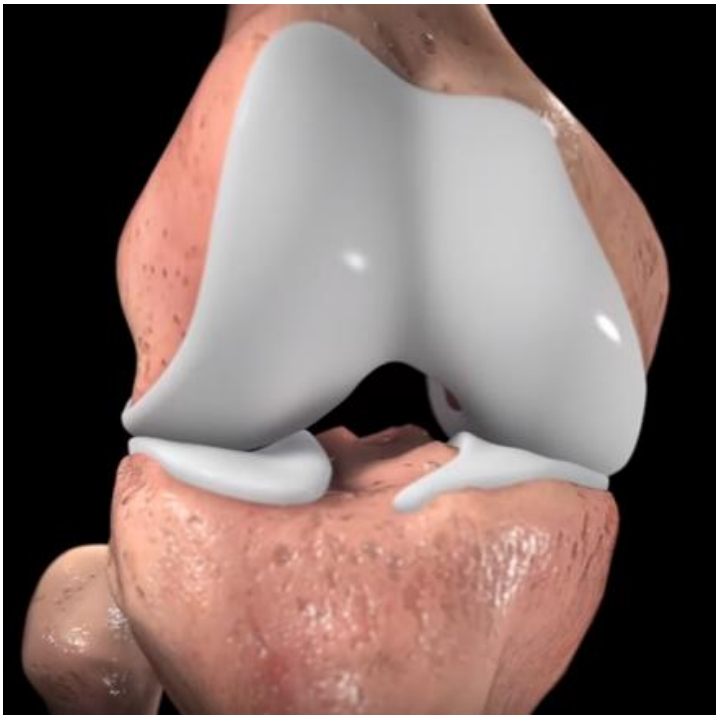

Figure 1: representation of human knee articular cartilage.

From a biological point of view, articular cartilage is composed of a dense extracellular matrix (ECM) with a sparse distribution of highly specialized cells named chondrocytes.[2] Conversely to the majority of the body tissues, chondrocytes are the only one cell type within the tissue, accounting for 1% of the total tissue volume. [1] They are devoted to the development and

maintaining of the tissue integrity, but unfortunately the poor proliferation ability and the low anabolic activity limited the repair of damages. Those features are due to the lack of innervations, lymphatic stream and, most importantly, blood stream, leading the chondrocytes metabolism to be dependent upon diffusion of oxygen, nutrients and other regulatory factors from the synovial fluid and subchondral bone through the ECM. Such diffusion is aided by the joint motion and load, which create the flow of extracellular fluid in and out of the tissue. [1] The ECM is mainly constitute by fibers of collagen type II, built to last forever, proteoglycans (*e.g*. aggrecan), and other non-collagenous protein present in lesser amount that undergo variable turnover. The organization of chondrocytes and ECM within the tissue varies greatly with respect to the *zone* take into consideration: *superficial*, *middle* or *deep zone*. Approximately the 10-20% of the thickness of articular cartilage is composed by the *superficial* layer in which chondrocytes are present in a relatively great amount showing a flattened morphology, surrounded by collagen fibers (type II and IX) aligned parallel to the surface. This layer is in deep contact with the synovial fluid, allowing the passage of nutrients and protecting the inner zones from shear stresses. Moreover, together with the synovial fibroblast, the superficial chondrocytes secrete lubricin, the latter helping the lubrication of the joint surface. The *middle zone* is the thicker layer, counting for the 40-60% of the articular cartilage volume. In this zone, chondrocytes have a spherical shape and a lower density; moreover the *middle zone* is characterized by the presence of proteoglycans and collagen fibers that become more thicker and are organized obliquely for resisting to compressive forces. The *deep zone* represents the remaining 30% of the cartilage volume. Chondrocytes are arranged in columns, parallel to the collagen fibers and perpendicular to the joint line. The large diameter of the collagen fibers in addition to their radial disposition, the increase of proteoglycans population in the ECM and a decrease of water content provide the greatest resistance to compression. The collagen fibers of the *deep zone* are anchored to the subchondral bone by a calcified layer formed by hypertrophic chondrocytes surrounded by apatite and calcified salt. In addition to this classification, three main *regions* can be distinguished within the cartilage tissue, based on the distance from chondrocytes.

The *pericellular region*, mainly composed by proteoglycans, which surrounds chondrocytes that are arranged in chondrons (single or clusters groups of chondrocytes), and it is responsible for the initiation of the signal transduction cascade. The *territorial region* borders to the *pericellular region*, protecting the chondrocytes from mechanical stresses thanks to the distribution of collagen fibers in a basket network around the cells. The *interterritorial region* is the most distant region with the greatest biomechanical properties, thanks to the presence of both large collagen fibrils and proteoglycans.

1.2 Osteoarthritis

Under normal condition, chondrocytes retain a very similar differentiation status through all the adulthood, defined as *immature*. In this state, chondrocytes do not proliferate and are devoted to remodel and maintain the ECM before entering the proliferative state, becoming hypertrophic and terminally *mature*. The absence of blood stream, lymphatic stream and innervations is at the root of the poor proliferation and regeneration ability of the tissue. Unfortunately, articular cartilage is subjected to numerous traumas that can occur during life from long term wear, repetitive mechanical loading and physical injuries, but also inflammatory and genetic diseases can arise. As a result, a progressive and irreversible degeneration of the cartilage could lead to changes also in the adjacent synovial and bone tissue resulting in a group of diseases referring to osteoarthritis (OA) and rheumatoid arthritis (RA).

Figure 2: representation of the degeneration of knee articular cartilage. Bone is exposed, promoting knee pain and further damages.

Worldwide, more than 10% of men and 18% of women older than 60 years is estimated to be affected by OA [3] which represents the leading cause of human pain and disability in the United States [1], and the most common degenerative disorder affecting one or multiple diarthrodial joints (hand, knee and hip joints). Women are more prone to develop structural osteoarthritis respect to man at any give age > 50 years, with the sex difference most pronounced for knee and hand OA.[4] Despite the great diffusion, the risk factors and the pathophysiology of this disease are not completely elucidated. Apart from sports trauma, accident and heavy work, the increasing of life expectation and obesity are recognized as the leading causes in developing OA. Regarding obesity, Jones and co-workers [5] demonstrate that children that are physically active present a higher volume of cartilage with respect to those who are more sedentary, thus concluding that physical activity is associated with a beneficial effect on knee articular cartilage in healthy adults, whereas a wrong diet can increase risks for OA. Some genetic traits are associated with OA of the hand and the spine, whereas loci associated with knee OA are not yet discovered. [6] [7] The discovery of a potential involvement of specific genes could lead to the use of selective biomarkers that could be

integrated with the preventive intervention for higher efficacy of the therapies, improving patient outcome. The evolution of the disease is usually slow, with symptoms that could include pain, structural abnormalities, transient morning stiffness, crepitus on joint motion and disabilities, even if the intensity of the pain vary greatly between patients and may depend also from the affected joint.

1.3 Molecular mechanism of joint degeneration

As mentioned hereinbefore, chondrocytes represent the only cell type present in the articular cartilage tissue. Under physiological conditions, chondrocytes exhibit no mitotic activity, while they maintain an appropriate turnover of proteoglycans and glycosaminoglycans. Collagen fibers instead are produced to last forever, so their turnover is minimal (limited). Chondrocytes exist in a low-oxygen tension environment, and intracellular survival factors, such as hypoxia-inducible factor 1α, are required for maintenance of homeostasis and adaptation to the mechanical environment. [8] Mechanosensitive-receptor and primary cilia, atop the cell membrane, are useful tool to capture physical stimuli and monitor the external environment. Normally, the collagen network provides tensile strength while the retention of water between the negative proteoglycans chains provides great compressive resilience. With aging, the secretion and the turnover of molecules decrease, as noticed also in OA in which a final complete remodeling of the whole joint occurs. The initial erosion, or fibrillation, of the ECM involves the *pericellular region* around chondrocytes, that is degraded, leaving the receptor of the cell membrane exposed to components of the *interterritorial region* deregulating chondrocytes functions *via* cell surface receptors, including integrin and discoidin domain receptors. [4] The process evolves in a deep fissuring associated with exfoliation of cartilage fragments, depletion of proteoglycans and collagen fibers, ultimately causing the exposure and expansion of the calcified cartilage.

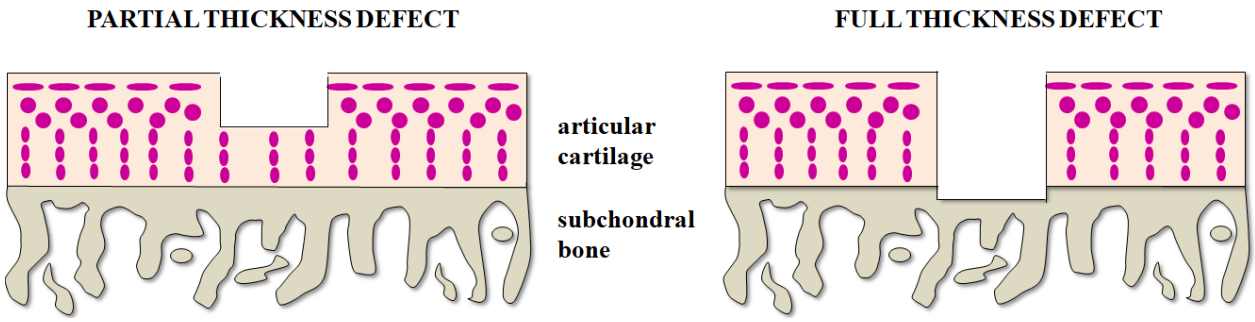

Figure 3: schematic representation of partial thickness defect (left) and full thickness defect (right). Partial thickness defects involved only the articular cartilage and may be, in some extent, repaired by native chondrocytes. In full thickness defects there is the exposure of the subchondral bone. Bone marrow stromal cells invade the joint defect and differentiate forming a fibrous cartilage that is not able to restore the native tissue.

When the damage arrives to the underlying bone, there is the penetration of vascular elements from bone marrow, sensory and sympathetic nerves. Mesenchymal stromal cells from bone marrow arrive at the injured site, and they undergo a differentiation process, leading to the formation of fibrous cartilage, the latter lacking of the physical and mechanical properties of the native tissue. During the later stage of OA, matrix degradation continues with chondrocytes that increase the production of metalloproteinases and aggrecanases and other proteins related to hypertrophy. Both in senescence and OA there is the increase of reactive oxygen species (ROS) production and the up-regulation of gene expressing proteins associated with inflammation. The pro-inflammatory mediators act both in an autocrine and paracrine pathway, thereby deregulating chondrocytes functions and stimulating the adjacent synovium in maintaining a proliferation state and a pro-inflammatory response. As osteoarthritis is a whole joint disease, changes occur also at bone level. Normally, bone is a highly structured material whose homeostasis depends on the balance between the activity of osteoclasts and osteoblasts, and the biomechanical factors that are involved in this process of remodeling of the bone. The progressive degradation of articular cartilage and the narrowing of the joint space lead to the direct contact between opposite bones causing pain. The altered balance between osteoblasts and osteoclasts activity alter the mineralization state, with the increasing of fissuration and decreasing of bone mass. Bone lesions

result in further subchondral bone cystis, bony outgrowths (osteophytes, localized on the joint margins), bone marrow edema and fibrosis. Inflammation of the synovial membrane, synovitis, is also present in late stages of OA. The synovial membrane becomes semi-permeable with further infiltration of lymphocytes T and B and hyperplasia. Proteinases that are released by chondrocytes lead to the generation of pro-inflammatory cartilage degradation products, which act as damage associated molecular patterns (DAMPs). DAMPs interact with Toll-like receptors and they act on the adjacent synovium to induce inflammation, that in turn generates additional pro-inflammatory and catabolic products, that feedback on the chondrocytes to further deregulate their functions. [4]

1.4 Current therapies

Nowadays there are no safe and complete approaches in the repair of cartilage defects and arthritic diseases. Personalized management strategies are customized on patients presenting cartilaginous defects in which cartilage and the surrounding tissues are not irreparably damaged. Patients experienced a multidisciplinary approach involving weight management, the maintaining of muscle mass and education for an healthy life. Those indications are associated with less pain and better functional outcomes. Patients are encourage in achieving goals, their progresses are followed and the therapy recalibrated based on patient improvements. In association with self-management, pharmacological therapies are proposed in patients with OA. Paracetamol and topical or oral nonsteroidal anti-inflammatory drugs (NSAIDs) are standard first line therapies. Also cyclooxygenase 2 (COX2) inhibitors are common pharmacological agents for the treatment of OA, whereas opioids are used only in few countries. Other procedures aimed at treating the symptoms deal with intra-articular injections of hyaluronic acid solutions, or in case of great pain, intra-articular injection of corticosteroids. If self-managements and pharmaceutical treatments fail to improve the life quality of patients, surgical procedures - based on the severity of the situation - are used. Arthroscopy lavage and debridement are used in the early stage of osteoarthritis. Both approaches involve the removal of cartilage fragments and debris of damage tissue during

arthroscopy to improve the mobility of the joint and alleviate the pain. These kind of approaches do not induce the repair of cartilage defects and the pain relief presents variability in the duration.

Figure 4: surgical procedure for the repair of a knee articular cartilage defect.

Arthroscopy approaches aimed at repairing cartilage damages are abrasion arthroplasty, Pridie drilling and microfracture. These procedures gain advantage from the full thickness defect in which there is the drilling and exposure of the underling subchondral bone and bone marrow, obtaining access to the vasculature and stimulating the bleeding. The clinical outcomes of these procedures are unpredictable, and in some cases the formation of the blood clot lead to the development of a fibrous cartilage tissue, which could not sustain the mechanical properties of the native tissue. [9] [10] In cases of more severe symptoms, soft tissue grafts are employed. Periosteum (or perichondrium) is harvested and implanted in a full thickness defect. It was demonstrated that both chondrocytes precursor cells, present in the cambial layer, and the mesenchymal stromal cells, derived from the exposed suchondral bone, are able to contribute to the repair of cartilage defects. [11] Mosaicplasty is a procedure that refers to the removal of a

cylindrical plug of osteochondral tissue from non-load bearing region of the articular cartilage of the patient, or from cadaveric donors. Several studies demonstrate good outcomes following to this procedure [12] [13] [14] , with decrease of pain and improved joint function, but the fact that the grafted tissue derived from a non load-bearing zone rise question about the ability to withstand mechanical forces. Laszlo Hangody et al. [15] reported 10 years of clinical successful autologous osteochondral mosaicplasties. Sixty-nine of eighty-three patients who were followed arthroscopically showed congruent gliding surfaces, histological evidence of the survival of the transplanted hyaline cartilage, and fibrocartilage filling of the donor sites. However, mosaicplasty can be used for lesion ranging from 1 to 4 cm^2, whereas the implantation of multiple osteochondral plugs in bigger defects lead to higher rate of donor-site morbidity. Grande et al. [16] described the first use of *in vitro* autologous cultured chondrocytes prior to grafting. Autologous chondrocyte implantation is indeed a valid option for lesions ranging from 2 to 12 cm^2, and when mosacplasty and other arthroscopy fail to decrease patient's pain. A biopsy of healthy cartilage of the patient is made and chondrocytes isolated *via* enzymatic methods. Chondrocytes are cultured for 14 days in order to increase the initial cell number of 20-50 times. The monolayer is then trypsinized and cell suspension included into a periosteal flap and injected into the defect. Numerous other studies [17][18][16] reported a great success of this procedure, with the formation of a fully integrated hyaline cartilage. Still the procedure is subjected to minimal immunological response and variability of outcomes based on patient's clinical history and limitations such as unmatched mechanical property of the repaired region, lack of integration, and donor-site morbidity. When all the medical interventions named before failed to improve patient life and a persistent degeneration of articular tissues continues, a total joint replacement using prostheses is needed. Of course, patient age should be considered, given the fact that prostheses last only 15 years.

1.5 Tissue Engineering of articular cartilage

Giving the uncertain outcomes of the procedures described before for the restoration of a natural hyaline cartilage, researchers are focusing their attention on the development of new strategies for this aim. The bone, articular cartilage and the thin region of calcified cartilage in between form a biocomposite material, which is uniquely adapted to transfer loads during weight bearing and joint motion [19]. Therefore, a tissue engineering approach could be used in order to restore such complexity of the tissue. Tissue engineering (TE) emerged in the mid 80's thanks to the efforts of Robert Langer and Joseph Vacanti [20], who precisely described (and define) the aim of Tissue Engineering. The main idea is to combine cells and signaling molecules within a biomaterial (scaffold, hydrogel, membrane), the latter should be able to fully sustain the growth of the embedded cells. The biomaterial must be able to integrate with the native environment and degrade following the regeneration of the tissue; moreover it should preserve the mechanical properties of the surrounding tissue. Besides, the cytotoxicity must be kept into consideration.

In order to completely restore the articular cartilage tissue, two types of cells are currently used: chondrocytes and mesenchymal stromal cells. Chondrocytes harvested from articular cartilage of the patient are the best candidate, producing cartilage specific-ECM. Unfortunately the isolation is quite difficult and there is the risk of donor site morbidity. Nasoseptal or auricular chondrocytes are investigated as potential substitutes of articular chondrocytes, since they are easier to harvest, associate with lower donor-site morbidity, and possess a higher proliferation rate [21], even if there are some doubts about their ability to produce a hyaline cartilage capable of sustaining the mechanical stresses that occur at the joint site. Moreover, articular, nasoseptal and auricular chondrocytes need precise culture conditions such as a 3D environment, low oxygen tension, and they should not fall into many expansion cycles *in vitro*, otherwise they could lose their classical phenotype. Mesenchymal stromal cells (MSCs) are the main alternative to the use of chondrocyte for articular cartilage repair. This kind of cells are able to differentiate into the three main

mesechymal cell lines (ostecytes, chondrocytes and adipocytes), maintaining their multipotency after numerous cell passage in culture. Moreover they can be harvested from different sites (bone marrow, adipous tissue, tooth) which do not affect negatively the said damaged cartilage. Both autologus and non-autologus MSCs could be used because they generally do not express molecules of the class II of major histocompatibility complex (MHC-II), responsible for immune rejection. [22]

Cells are seeded into a 3D material that should mimic the native environment of the articular cartilage. Both natural and synthetic polymers are currently used in order to develop specific biomaterials (*e.g.* hydrogels, solid dried scaffolds, micro-beads or nanoparticles) that could sustain the cells growth or deliver specific factors that could stimulate the proliferation or the differentiation of the cells. Natural derived polysaccharides (*e.g.* chitosan, alginate, carrageenan and chondroitin sulfate) are hitherto widely used for their versatility, tunable properties biocompatibility, biodegradability, non-toxicity and for their economical benefits. Several TE approaches are investigated for cartilage repair and regeneration. As for transplant, also biomaterials can be subjected to rejection, hence Yuan and co-workers [23] investigated the ability of a collagen based hydrogel of reducing the immunogenicity when MSCs or chondrocytes were seeded, underling how the presence of a natural molecule, *i.e.* collagen, can mimic the ECM of the articular cartilage, decreasing the rejection possibility. Three-dimensional culture of infant chondrocytes and MSCs from human hip seeded in a polyglycolic acid – fibrin – platelet rich protein (PGA-fibrin-PRP) scaffold initiates re-differentiation that is accompanied by the induction of typical chondrocytes and mesenchymal markers such ad collagen II and cartilage oligomeric matrix protein (COMP). [24] Again, TE does not encompass cells and scaffolds, but the delivery of growth factors or active molecules able to sustain the regeneration of the tissue is mandatory. Often, different release kinetics of said molecules is needed. Nanostructured systems may guarantee to achieve this goal. Hence, the combination of such nanosystems with scaffolds could be potentially

of paramount importance. Several nanocarriers have been investigated for this purpose, but polymeric nanoparticles based both on synthetic or natural polymers remain largely preferred. This integrated system offers an adequate presentation of the bioactive molecule to the surrounding cells and a controlled release over time [25].

Currently there are some commercially available products for cartilage repair that are based on a TE approach as Novocart®, Cartipatch ® or BioCart™II. [26] Nevertheless, due to difficulties in evaluating the quality of the engineered cartilage, including its safety, cost-effectiveness, and complications in the procedure, most of the new developments in cartilage TE have yet to translate into the clinical market.

1.6 Complex coacervates

Complex coacervation refers to a phenomenon in which two oppositely charged polyelectrolytes (PE) are combined to form a ionically cross-linked coacervate in the nano/micro size range. Under appropriate conditions it is obtained a liquid-liquid phase separation, resulting in a biphasic system in which the coacervate-rich phase is in equilibrium with the PE-poor solution phase. In the recent years, this system was widely investigated for the delivery of therapeutics molecules. Several examples of PE coacervates are reported in the literature. For instance, chitosan/nucleic acid polyplexes were designed for the in vitro delivery of RNA or DNA in mammalian cells. [27][28] Similarly, hybrid PEGylated nanoparticles formed *via* complex coacervation mechanism have shown to enhance the *in vivo* gene transfection efficiency compared with traditional carriers. [29] Butyrate loaded chitosan/hyaluronic acid nanoparticles have demonstrated excellent anti-inflammatory properties, decreasing ROS production by TNF-stimulatated neutrophils *in vitro*. [30] Furthermore, poly(ethylene argininylaspartate diglyceride) and heparin coacervates were loaded with bone morphogenetic protein 2 improving the osteogenic potential of muscle-derived stem cells. [31]

The phase separation of oppositely charged macromolecules can be influenced by ionic strength (salt concentration), pH, temperature, stoichiometry of PEs involved in the process, molecular weight and charge density of polyelectrolytes, chain flexibility, and polyion concentration. [32] By appropriately tuning these features, coacervates efficiently encapsulate proper payloads [33] [34] and release them in a pH dependent fashion, by degradation, or by diffusion, depending on the desired purpose.

1.7 Hydrogels

A hydrogel is a 3D network of polymer chains able to absorb a great water amount. Hydrogels can be composed up to 99% of water, depending on the polymer content. The high water content offers a good hydrophilicity that allows cells attachment and an optimal integration with the surrounding tissue. From a mechanical point of view, hydrogels may behave as purely elastic or viscoelastic materials, depending on the type of network and water movements into the polymeric matrix when exposed to a stress. The stiffness of the material can be modified by changing the polymer concentration, chain entanglement, the ligand density and network porosity in order to obtain appropriate mechanical properties. In fact, cells are influenced by several parameters such as rigidity, elasticity, roughness, hydropilicity and molecular pattern of the hydrogel surface. All these features are important when the bulk material for the hydrogel formation is considered. Both synthetic and natural polymers are used for the preparation of hydrogels, but natural biopolymers offer particular advantages as they are abundant, low cost, biocompatible, bioactive and can mimic the ECM of the natural tissue. Hydrogels gelation is achieved by either physical or chemical cross-link methods. The first approach involves the formation of weak interactions within the polymer networks (*e.g.* ionic crosslink or H-bonds), whereas chemical cross-linking methods form strong bonds between polymer chains. [35] The complexation of the guluronic-units of alginate with divalent cations is an easy approach for the preparation of different forms of hydrogels that have been used in the biomedical field for cells encapsulation [36], or delivery of therapeutic molecules.

[37][38][39] Furthermore, mechanical and biological properties of chitosan hydrogels, fabricated using multivalent anions such as tripolyphosphate (TPP) or pyrophosphate (PPi), have been extensively investigated. The good homogeneity of the system and the possible colonization by cell lines represent very important features for the co-delivery of cells and growth factors in cartilage regeneration. [40][41] Recently, the behavior of a lactose-modified chitosan in the presence of borax as cross-linking agent was studied, shedding light on the marked non-linear behavior depending on the amount of borax added to the system. Such transient reticulation between the polymer and borax results in a mechanical performance that mimic the behavior of the macromolecules composing the ECM of natural tissues. [42] Stimuli-sensitive hydrogels have also been explored for site-specific drug release. Thermosensitive hydrogel of chitosan/beta glycerophosphate displayed a tunable sol-to-gel temperature from 35 to 56 °C, which can be controlled by changing the composition, and found possible applications in the wound healing field. [43][44] Moreover, thermosensitive hydrogel employed in the tissue engineering of articular cartilage can be injected, limiting the possible risk of a surgical procedure.

1.8 Hyaluronic Acid

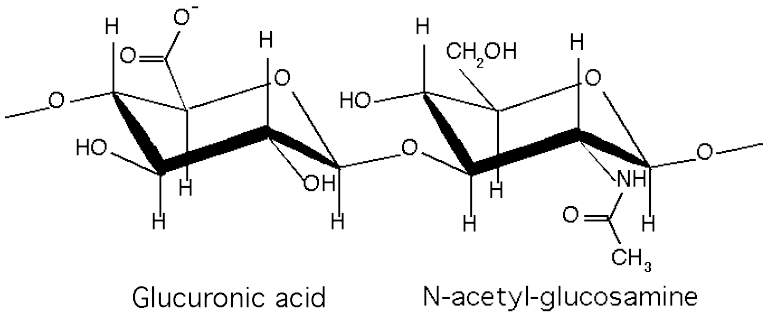

Figure 5: representation of the two monomers forming hyaluronic acid polymer.

Hyaluronic acid (HA) was first discovered in 1934 by Karl Meyer and John Palmer, who isolated it from the vitreous body of a cows' eye [45]. After that Endre Balazs developed a method

to isolate hyaluronic acid from the rooster comb, and nowadays it can be biotechnologically produced using several bacteria, *e.g. Bacillus Subtilis*. From a chemical point of view, hyaluronic acid (also known as hyaluronan) is a linear polysaccharide composed of a very stable structure of repeating disaccharides units of *N*-acetyl-D-glucosamine and D-glucuronic acid. Hyaluronic acid is a high molecular weight non sulphated glycosaminoglycan, and the only one produced outside the Golgi. The synthesis of HA occurs at the plasma membrane level and it is extruded directly in the ECM. Its lubricant and viscoelastic properties were first noticed, deriving from its great water retention. Deeper investigations of HA nature underlined its emerging role in several biological processes such as embryogenesis, signal transduction, [46] cell migration, proliferation [47], and its scavenger activity against free radicals. HA is present in several human tissues, in particular skin, eye, synovial and articular cartilage. Its diffusion in different tissues and its stunning properties have driven the development of several products based on this macromolecule. Commercially available HA-based products like Hyalomatrix and Hyalosafe are medical devices dedicated to wound healing [48], whereas Restylane and Hylaform are fillers used in plastic surgery [46]. HA has raised great interest in the field of viscosupplementation for the treatment of arthritic and rheumatic problems, thanks to its pivotal role as component of the ECM of cartilage and as lubricant in the synovial fluid. Hyaluronic acid usage in knee OA is conditionally recommended by the 2012 ACR guidelines in individuals with knee OA who are > 74 years old, with symptoms refractory to standard pharmacological treatments. [4] Modified HA such as HYAFF® (Fidia Advanced Biopolymers, Abano Terme, Italy) in combination with mesenchymal stromal cells are suitable for the development of scaffolds for articular cartilage regeneration [49] [50] [51] [52], giving promising input for the TE field.

1.9 CTL: a Lactose-modified Chitosan

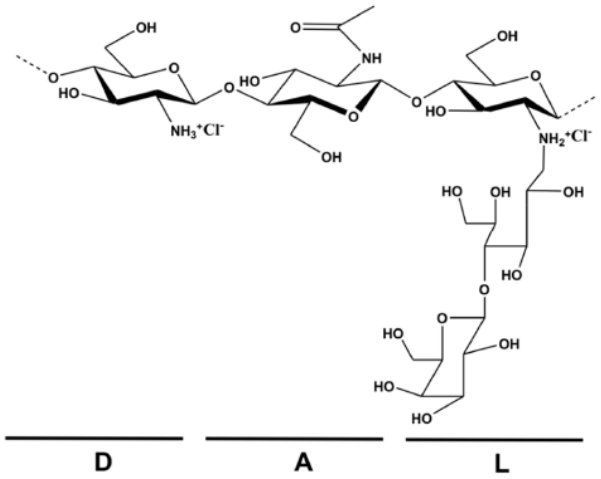

Figure 6: lactose modified chitosan (CTL): glucosamine (D), N-acetyl-glucosamine (A) units and lactitol side chain (L).

Chitosan is a linear polysaccharides derived from deacetylation of chitin, a naturally abundant mucopolysaccharide, structural component of the cell wall of crustaceans, insects and fungal,[53] and the second most abundant polysaccharide on earth. Chitosan is almost the only cationic polysaccharide present in nature [54], and this unique property is of great interest for several applications from food packaging to biomedical ones. It is well known that chitosan has muco-adhesive properties and it is also biocompatible, biodegradable and possesses anti-bacterial and anti-inflammatory activities. Although biotechnologically relevant, chitosan can be solubilized only at low pH and it is poorly soluble at neutral pH conditions. This is reasonably valid if classical commercial chitosans with medium to high molecular weight (MW) and fraction of acetylated units (F_A) < 0.4 are considered, albeit the solubility at neutral pH can be sensibly improved by reducing MW thereof in the order of few consecutive sugars, *i.e.* showing a degree of polymerization (DP) < 10. In order to overcome these limitations evidenced for medium to high MW and low acetylated chitosans, several chemical modifications may be undertaken. Quaternized derivatives as *N*,*N*,*N*-trimethyl chitosan chloride presents a much higher solubility in water, whereas trimethylation of chitosan improved the muco-adhesive properties. Furthermore, chitosan could be alkylated for DNA delivery [29] or modified with the addition of different sugars. Yalpani et al., [55]

explored several modifications of chitosan with the addition of pendants. In our laboratory, we are interested in studying a lactose-modified chitosan firstly named “Chitlac” and then called CTL. This highly branched polysaccharide gained biological significance in terms of good solubility at neutral pH, cell-stimulation effects toward bone and cartilage cells and specific ligand-receptor interaction mediated by lectins. [56] [57] CTL has been investigated for its bactericidal and non-cytotoxic effects in combination with silver nanoparticles [58], as a bioactive coating of BisGMA/TEGDMA thermoset materials [59], for the possibility of preparing binary polymer mixtures with an opposite charged polysaccharide like alginate, [57] to create three-dimensional hydrogels able to sustain chondrocytes growth [60], and more recently used in combination with tripolyphosphate to create highly monodisperse nanoparticles [61]. Marcon *et al*. investigated the involvement of Galectin-1 as a molecular bridge between CTL and chondrocyte cell surfaces, demonstrating the bioactive role of such polymer. [62] Furthermore, the mechanical properties of CTL upon treatment with boronic acids derivatives such as boric acid was explored, showing peculiar dilatant behavior in conditions of steady flow and oscillatory state, [63] that rose interest in our group in order to further explore this branched polysaccharide for applications in the TE field.

1.10 Alginate

Among the several natural biopolymers that are used for TE application, alginate is one of the most versatile. From a chemical point of view, the name alginate refers to a whole family of natural, linear copolymers, first described by the British chemist E.C.C. Standford in 1881[64], composed by blocks of (1,4)-linked D-mannuronate (M) and L-guluronate (G) residues. Such residues are distributed differently, based on the type of alginate considered.

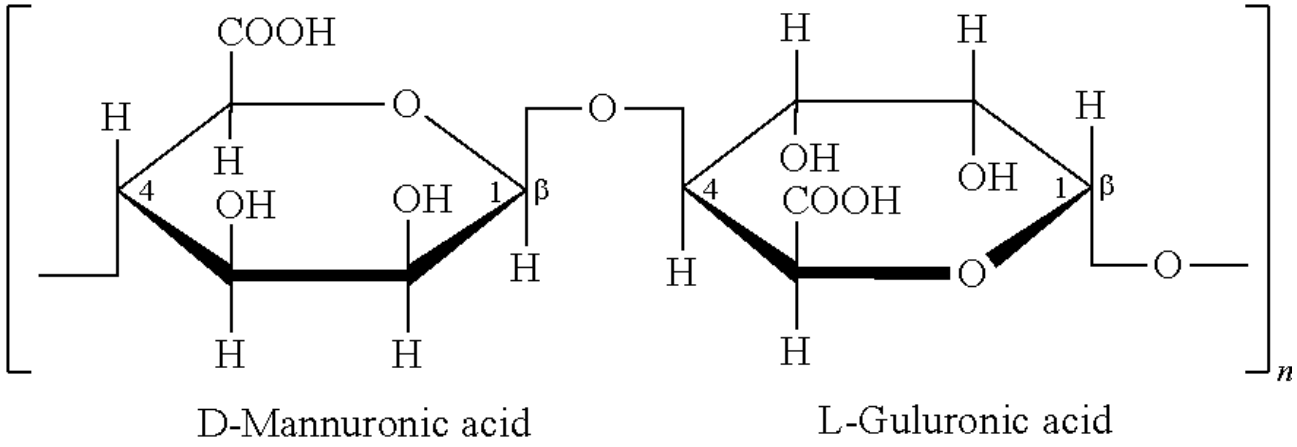

Figure 7: schematic representation of the monomers composing Alginate.

This copolymer is mainly obtained from brown algae, bacteria like *Pseudomonas aeruginosa*, and, nowadays, it is also biotechnologically produced. The abundance of sources of alginate has decreased greatly its price, making this polymer widely used from food industry to tissue engineering materials or drug delivery systems. The use of alginate in several applications derived from its good scaffold-forming properties thanks to the ability to form stable gels in the presence of divalent cations, such as Ca^{2+}, which are bound by the guluronic monomers in a highly cooperative manner, with the consequent formation of structures called "egg-boxes", described for the first time Grant *et al.* in 1973. [65] Alginate displays an optimal biodegradability, biocompatibility and non-immunogenicity, these last two related to the lack of interaction with proteins and cells. In order to improve the affinity of the cells for alginate, its properties can be tailored with the addition of small peptides or bioactive molecules. Alginates constructs can be easily shaped based on the final application. Currently, alginate is used in combination with hydroxyapatite to obtain composite materials for bone regeneration [66] [67], to prepare beads for efficiency encapsulation of mesenchymal stromal cells [68] or used in combination with chitosan to form polyelectrolyte complexes membrane for wound healing [69] and nanoparticles for drug delivery systems. [70][38]

1.11 Chondroitin Sulfate

Chondroitin sulfate (CS) is a sulfated glycosaminoglycan composed by a linear polysaccharide chain of repeated units of *N*-acetyl-galactosamine and glucuronic acid. CS is one of the major components of the extracellular matrix of several connective tissues, including articular cartilage, and in this precisely tissue contributes to its resistance and elasticity.

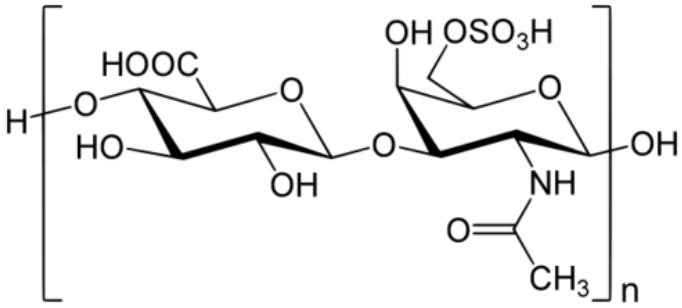

Figure 8: schematic representation of chondroitin sulfate.

Nowadays, CS is obtained from bovine, porcine or shark cartilage, and the safety of this drug has allowed its use in medicine from many years, alone or in combination with other compounds. In particular its chondroprotective properties attracted great interest as potential agent against arthritic and rheumatic disorders. It was shown that CS possesses anti-apoptotic, anti-oxidant and anti-inflammatory properties by inhibiting *in vitro* the synthesis of several pro-apoptotic and inflammatory mediators, and *in vivo* by reducing synovitis in collagen-induced arthritis in mouse. [71] Moreover, CS presents an anabolic effect by increasing the synthesis of collagen type II and proteoglycans and downregulating the expression of metalloproteinases which usually destroy the ECM. [72] Chondroitin sulfate is reported as a symptomatic slow-acting drug used as ground therapy for OA, [73] and can be used alone via oral administration or as intra-articular injection in order to reduce the administration of NSAIDs and the consequent risk of gastro-intestinal tract erosion and renal failure. However, CS is also applied in the TE field contributing to the formation of hydrogels and scaffolds in combination with chitosan and hyaluronic acid [74] or in combination with chitosan for the delivery of hydrophilic molecules.[75][76][77]

2. AIMS

The work of this three year thesis aimed at the development and characterization of a biomaterial for cartilage repair that combines an intrinsic capability to promote tissue regeneration with a long-term sustained-release of bioactive molecules. The biomaterial will be designed in form of an hydrogel prepared with bioactive polymers encapsulating polysaccharides-based coacervates able to load small molecules.

A schematic overview of the project is reported in Figure 9: the main idea was to combine micro/nano-size delivery systems with a bulk matrix, presenting similar characteristics of those of articular cartilage. As mentioned before, such tissue-engineering application needs the use of appropriate materials that should be devoid of toxicity and, possibly, with intrinsic bioactivity with respect to the target tissue.

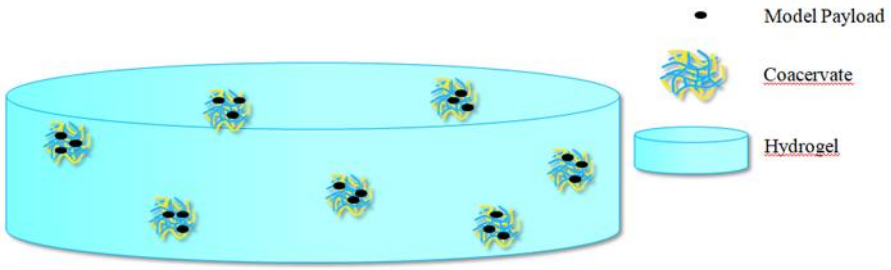

Figure 9: schematic representation of the final biomaterial obtained during the three years of work

The research activity developed through the following intermediate objectives:

- Analyses of the miscibility of two oppositely charged polymers (CTL and hyaluronan) under different conditions (namely: ionic strength, polymer mixing, molecular weight of the polymer, pH, weight fraction of the polymer).
- Formation of stable complex coacervates between CTL and hyaluronan, providing novel insights and further prospective in the field of coacervates between oppositely charged polyelectrolytes.

- Evaluation of the loading capacity and the release kinetic of the coacervates system using a model payload (*i.e*. Dexamethasone).
- Evaluation of the possible biological contribution of the HA/CTL coacervates in the repair of articular cartilage.
- Preparation of a hydrogel based on polymers that could promote the repair of the articular cartilage.
- Embedding of the coacervates system into the hydrogel in order to obtain a long term sustained release of a model molecule.

3. EXPERIMENTAL SECTION

CHAPTER 1: Miscibility studies of HA and CTL solutions

3.1.1 Aim of the work

This first section of the thesis is dedicated to the miscibility studies between two oppositely charged polyelectrolytes, namely hyaluronic acid (anionic) and CTL (cationic), analyzing the main parameters affecting the transition from binary solution to complex coacervation. In particular, the key parameters investigated are: pH, weight ratio of the two polymers, ionic strength and molecular weight.

3.1.2 Materials and Methods

3.1.2.1 Materials

Sodium hyaluronates, HAs, at different molecular weight (see Table 1) were kindly provided by Sigea s.r.l. (Trieste, Italy). Two samples of the hydrochloride form of CTL (CTL60 and CTL47) with different fractions of lactose-modified glucosamine units (i.e. N-(1-deoxylactit-1-yl)), were provided by biopoLife s.r.l. (Trieste, Italy). They had been obtained from two different chitosan batches from Chitoceuticals Heppe Medical Chitosan GmbH, Germany. The viscosity- average molecular weight, Mv, of the starting chitosans were 360 000 for CTL47 and 380 000 for CTL60, respectively. According to the determined composition, the corresponding (derived) Mv values of the CTL derivatives were 760 000 and 910 000, respectively (see Table 2). The physical−chemical features of CTL samples are summarized in Table 2.

HEPES buffer, acetic acid, sodium acetate and sodium hydroxide were purchased from Sigma Aldrich Chemical Co. (Milwaukee, WI). Hydrochloric acid was purchased from Carlo Erba (Milano, Italy). Deionized Milli-Q water was used throughout.

HA sample	[η] (mL/g) pH 7.4	$\overline{M_v}$ pH 7.4	[η] (mL/g) pH 4.5	$\overline{M_v}$ pH 4.5
HA90	270	90 000	279	93 000
HA310	736	310 000	754	330 000
HA570	1210	570 000	1433	700 000

Table 1: Resuming table of the three HAs used with their intrinsic viscosity and viscosity-average molecular mass t at pH 7.4 and 4.5.

CTL sample	F_A	F_D	F_L	$\overline{M_v}$
CTL60	0.07	0.33	0.60	910 000
CTL47	0.12	0.41	0.47	760 000

Table 2: Chemical composition of CTL samples used in this study. FA stands for the fraction of acetylated units, FD for the fraction of deacetylated units and FL for the fraction of lactose-modified units. M̄v is the viscosity-average molecular mass of CTL samples, calculating on the basis of the corresponding M̄v values of the parent chitosans and of the values of FL.

3.1.2.2 Determination of Intrinsic viscosity for HAs and CTL

The intrinsic viscosity [η] of polymers used in this work was determined by means of a CT 1150 Schott Geräte automatic measuring apparatus and a Schott capillary viscometer. In the case of CTL60 and CTL47, the same protocol described in [78] was used. In the case of HA samples, a known amount of polymer was solubilized using NaCl 0.15 M as buffer solution. Subsequently, solutions were filtered through a 0.45 μm Millipore (Germany) nitrocellulose filter before the measurement. The intrinsic viscosity was calculated at T = 25 °C by analyzing the polymer

concentration dependence of the reduced specific viscosity $^{\eta_{sp}}/_{c}$ and of the reduced logarithm of the relative viscosity $^{\ln(\eta_r)}/_{c}$ calculated from Huggins (1) and Kramer (2) equations, respectively:

$$\frac{\eta_{sp}}{c} = [\eta] + k_1[\eta]^2 c \qquad (1)$$

$$\frac{ln\,\eta_r}{c} = [\eta] + k_2[\eta]^2 c \qquad (2)$$

where *k* and *k′* are the Huggins and Kraemer constants, respectively. The intrinsic viscosity values obtained were averaged. In the case of HA samples, the corresponding viscosity average molecular weight ($\overline{M_v}$) was calculated using the Mark-Houwink-Sakurada (MHS) equation (eq. 3)

$$[\eta] = K \cdot \overline{M_v^a} \qquad (3)$$

where *K* and *a* parameters correspond to 2.63 x 10^{-4} and 0.81, respectively.[79] The measurement of the capillary viscosity of the polymers were carried on also at pH 4.5 using 20 mM of AcOH/AcNa as buffer), conforming to the pH of subsequent miscibility experiments.

3.1.2.3 Miscibility studies of HA and CTL

HAs and CTL60 were dissolved separately in deionized filtered water, with a final concentration of 1.5 g/L. The polymers solutions were both prepared at two different pH value, namely 7.4 and 4.5. NaOH 0.1 M or HCl 0.1 M were used to adjust the pH of solutions to desired values before mixing. Polymers were then filtered through 0.45 μm filters. The two polymers were used for the preparation of a binary polymer mixture by mixing different amounts of a 1.5 g/L HA90 solution and a 1.5 g/L CTL60 solution, respectively, hence obtaining different HA weight fractions (*r*HA 0.15 – 0.25 – 0.50 – 0.75). A total polymer concentration of 1.5 g/L was kept. The binary solution was gently stirred for 20 min at room temperature before performing further analyses. In order to better investigate the behavior of such polymers under different conditions,

several parameters that could influence the mixing were taken into consideration: the dropped polymer during mixing, the molecular weight of the used polymers and the presence of supporting salt (*i.e*. NaCl 150 mM - 100 mM - 75 mM - 50 mM - 25 mM). Hepes and AcOH/AcNa buffers were used to stabilize the pH of solutions with increased ionic strength in the case of final pH 7.4 and 4.5, respectively. Supporting salt (NaCl)/buffer ratio equal to 15 was kept constant throughout the measurements.[80]

3.1.2.4 Turbidity measurements

The Transmittance (*T*) of the solutions both at pH 7.4 and 4.5 were measured at 550 nm with a Ultrospec 2100 pro spectrophotometer (Bioscience, England). As blank, the transmittance of separate polysaccharides and that of deionized water was measured as well. At least three replicates were recorded for each sample and the results were averaged.

3.1.2.5 ζ-potential measurements

Z-potential measurements were performed using a Zetasizer Nano ZS system (Malvern Instruments, Inc., Southborough, MA). Briefly, HA90 and CTL60 were dissolved separately at a final concentration of 1.5 g/L, pH 4.5, as described before. HA90 was added to CTL60 solution drop-wise, during stirring, in order to obtain solutions with different *r*HA (*i.e*. 0.15 – 0.25 – 0.50 – 0.75). Samples were diluted 1:10 in deionized filtered water before ζ-potential analyses. Values are reported as mean of three replicates. The same analyses were repeated for formulations prepared by dropping CTL60 into HA90.

3.1.2.6 Dynamic Light Scattering Analyses

Dynamic Light Scattering (DLS) measurements were performed using a Zetasizer Nano ZS system (Malvern Malvern Panalytical, Malver, UK), in order to evaluate the presence of coacervates in solutions. Such technique uses a monochromatic laser to detect spherical particles in

a solution. The incidence of the light with the particles in Brownian motion causes a Doppler Shift when the light hits the moving particle, changing the wavelength of the incoming light. This change is related to the size of the particle. [81]

The intensity of 173° scattered light (Derived Count Rate - kilocounts per second, kcps), the average hydrodynamic diameter and the polydispersity index (PDI) of the coacervates were considered. Coacervates solutions were diluted 1:10 v/v in filtered deionized water (pH 4.5) and DLS measurements were performed at 25 °C, analyzing each sample in triplicate.

3.1.3 Results and Discussion

During the first year of PhD, the behavior of two oppositely charged polymers mixed together was analyzed. Hyaluronan and CTL are biopolymers presenting beneficial effects on damaged articular cartilage. Studies on the preparation and characterization of binary or ternary mixtures of natural polyelectrolytes have been conducted in the past years[80], [82], [57], underling the importance of these polymers in the tissue engineering field. Both hyaluronan and chitosan, from which CTL derived, are natural polysaccharides widely used for biomedical applications. The structures of these polysaccharides resemble the biological network of macromolecules composing the ECM of a complex tissue such as the articular cartilage, whose role is to embed cells and provide structural, mechanical and biological support. The combination of these two different polysaccharides is expected to induce notable variation of the physical-chemical properties of the system, fostering the formation of complex coacervates. The formation of such system is influenced by parameters such as the pH of the solution, the ionic strength, the molecular weight of the involved polymers and the charge density. [32]

Several variables were investigated in order to better understand the behavior of these polyelectrolytes, thereby optimizing the coacervation process. First it was analyzed the miscibility of CTL60 and HA90 at physiological pH of 7.4 and very negligible ionic strength. More in detail, it was investigated the role played by polymer mixing (*e.g.* CTL60 solution dropped into HA90 solution during stirring - indicated as CTL60/HA90 - and vice versa, *i.e.* HA90/CTL60) and the final weight fraction of HA on CTL, simply indicated as *r*HA. The Transmittance (*T*) of the solutions was the analytical parameter for this study. As shown in Figure 10, the transmittance of the solutions prepared is comparable of that recorded for the single polymeric solutions and of pure distilled water used as control ($T = 100$). The absence of turbidity proves the mutual solubility of the two oppositely charged polysaccharides without apparent interactions, mainly due to the (almost) fully uncharged CTL at pH 7.4.

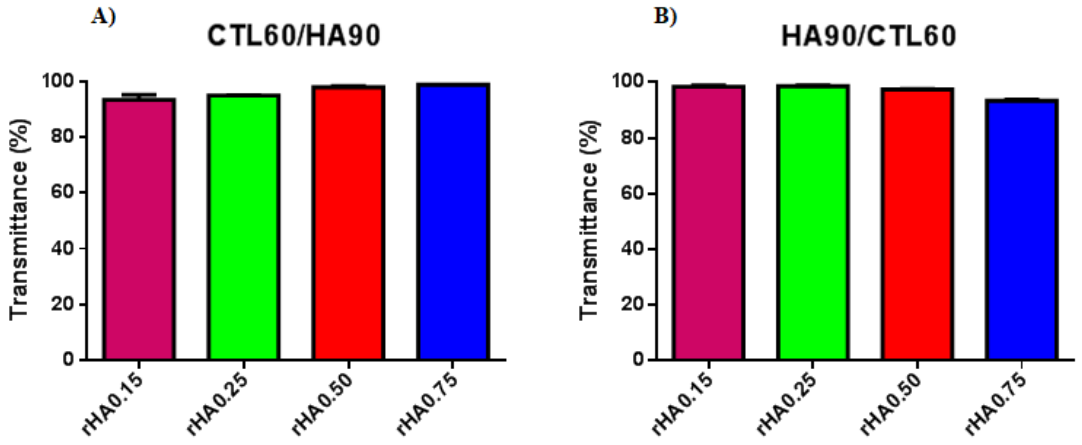

Figure 10: Influence of the pH, weight fraction and polymer mixing on the transmittance of binary mixturesprepared at pH 7.4. A) Formulations prepared by dropping CTL60 solution into HA90 solution. B) Formulations prepared by dropping HA90 solution into CTL60 solution. Results are reported as means (± SD, *n*= 3). Single polymers solution were used as controls.

The complexity of the system was increased by preparing binary mixture solutions in the presence of different amounts of NaCl as to vary the total ionic strength. In these experimental conditions no turbidity was detected for different weight ratio of the two polymers, since *T* values flattened around 100% (Figure 11). As anticipated above, the reason of these findings can be explained by the fact that the pK_a of primary and secondary amines of CTL60 are 6.69 and 5.87, respectively [56], hence they are mostly uncharged at pH 7.4. This means that inter-chain electrostatic interactions between the polysaccharides are strongly impaired. Therefore, in these conditions of pH (and ionic strength), no complex coacervation phenomena occurred. Similar behavior was already observed by Donati *et al.* [57] for a binary mixture solution of the polyanion alginate with CTL, where the mutual solubility was achieved at neutral pH and 150 mM of ionic strength.

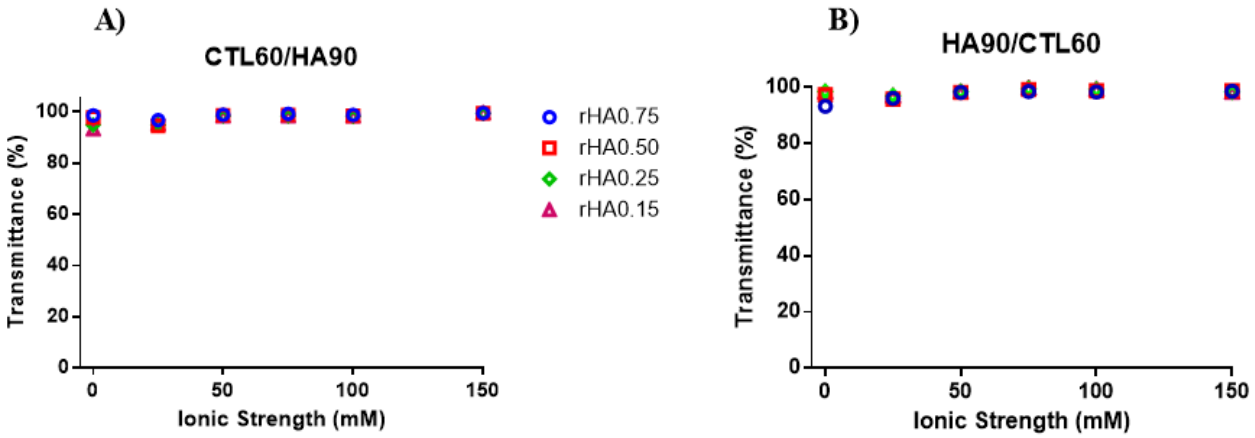

Figure 11: Influence of the ionic strength on the binary mixture solutions prepared at pH 7.4. A) Formulations prepared by dropping CTL60 solution into HA90 solution. B) Formulations prepared by dropping HA90 solution into CTL60 solution. Results are reported as means (± SD, *n* = 3). Single polymers solution were used as controls.

By mixing the polymer solutions at pH 4.5 and $I \sim 0$ mM, the onset of liquid-liquid phase separation was clearly highlighted by the increase of turbidity immediately after the polymer injection, which was then confirmed by a drastic decrease in the transmittance values (Figure 12A and 12B). The phase separation, with the consequent formation of coacervates, is entropically driven by the release of counterions and water molecules from polysaccharides, and by the onset of electrostatic interactions between CTL60 and HA90 at pH 4.5. In this conditions CTL60 is in fact expected being (almost) fully positive charged whereas HA showing around 70% of total repetitive (disaccharide) units negatively charged, given a dissociation degree, α, of 0.7 at said pH (pKa ≈ 3). The pH and the ionic strength of the solutions are therefore very important factors affecting the degree of ionization, hence influencing the complexation rate and phase separation of polyelectrolytes.[83]

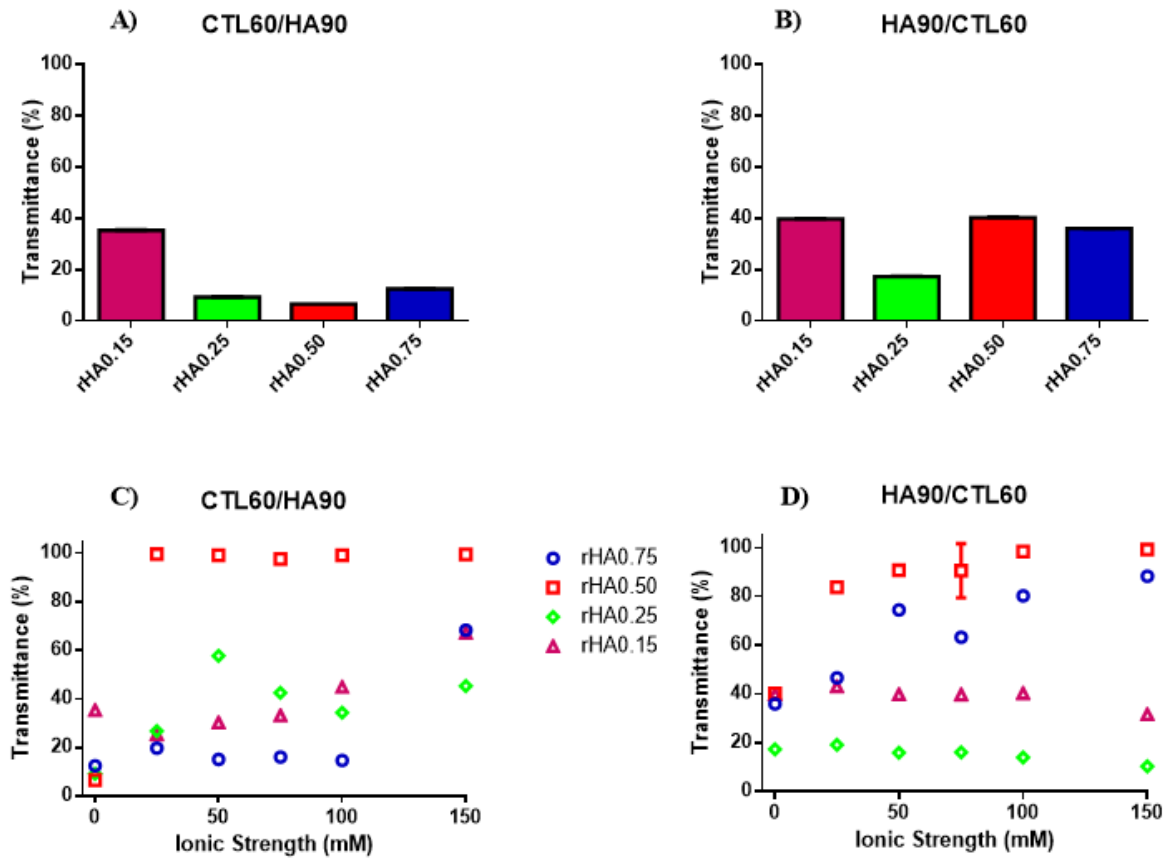

Figure 12: Influence of pH (A and B) and ionic strength (C and D) on the Transmittance of the binary mixture solutions of HA and CTL prepared at different *r*HA. A) and C) Formulations prepared by dropping CTL60 solution into HA90 solution. B) and D) Formulations prepared by dropping HA90 solution into CTL60 solution. Results are reported as means (± SD, *n* = 3).

In Figure 12C and 12D it is reported the analysis of the Transmittance, expressed as percentage, as a function of the ionic strength, for binary solutions prepared at pH 4.5 with different weight fraction of polymers. It can be observed that, conversely to the analyses at pH 7.4, the different formulations present a decrease of the transmittance values with a consequent increase of the turbidity of the system. However, some important aspects about the formulations have to be considered. First of all, the formulations prepared at pH 4.5 and without supporting salt not only manifested an increased turbidity, but also the presence of few micro-size precipitates was observed. By preparing the binary mixtures using the single polymeric solutions with the addition of NaCl a change in the behavior of the different formulation was noticed. Curiously, the formulations with *r*HA0.15 and 0.25 prepared by dropping HA90 into CTL60 did not display any

precipitate, when considering the all ionic strength range from 25 to 150 mM, and the turbidity suggests the presence of colloidal coacervates in solution.

Strikingly, it seems that the polymer mixing could influence the behavior of the final solution given the fact that when CTL60 is dropped into the HA90 solution at the same *r*HA cited above, the formation of precipitates occurred, albeit the turbidity of the systems was anyhow evident. By changing the content of HA in the final binary solution (*r*HA 0.75) it was observed that for formulations prepared by dropping CTL60 into HA90, a net turbidity of the system without the presence of precipitates for ionic strengths up to 75 mM was observed. As the ionic strength increased up to 150 mM, a pronounced increase of the transmittance of the formulations marked, at variance, the dissolution of coacervates and the formation of precipitates. Finally, when polymers were present at a weight ratio of 1:1 (*r*HA 0.50), *T* values were found very similar to that of pure water for all the ionic strengths analyzed, meaning that none complex coacervation occurred. However, large precipitates were present on the bottom of the vial. As already discussed, the charge ratio between the polyelectrolytes greatly influences the formation of complex coacervates. A qualitative representation of the physical behavior of the different formulation analyzed is reported in Figure 13.

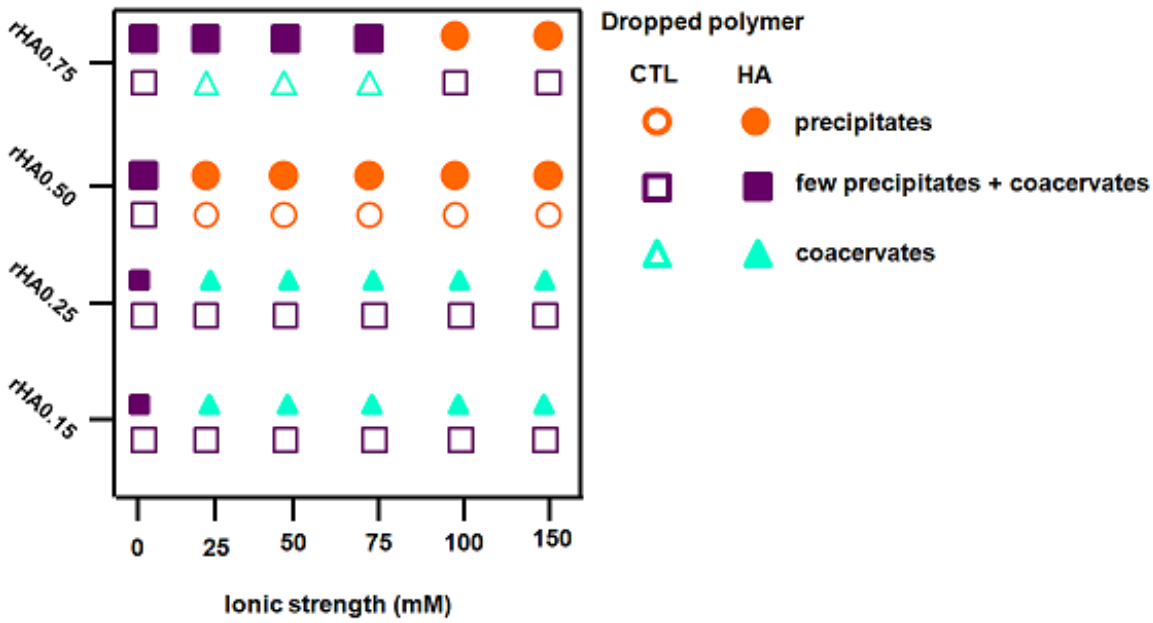

Figure 13: Schematic representation of the behavior of binary mixture solutions reported for different *r*HA as a function of ionic strength.

To better understand the behavior of the two polymers when mixed together, an evaluation of the theoretical ratio of positive on negative charges (+/-) with respect to *r*HA is reported (Figure 14A). By assuming that both HA and CTL are fully charged at pH 4.5, the charge ratio was found to scale with *r*HA according to the following power law, $^{(+)}/_{(-)} \propto rHA^{-1.7}$, thus indicating that the amount of positive charges decreases with the increasing of HA. In the case of *r*HA0.50, an almost stoichiometric balance between positive and negative charges ((+) / (-) = 0.96) was calculated, meaning that such a condition is at the root of aggregation and ensuing precipitation of colloidal coacervates. In fact, the loss of repulsive forces among complexes would increase the polymer mass per volume unit up to a certain limit, beyond which supramolecular assembly phenomena occur. The theoretical approach was verified experimentally by evaluating the dependence of coacervates surface charge on *r*HA. Z-potential analyses on formulations at different *r*HA were performed by DLS technique (Figure 14B). As expected, the decrement of the positive surface charge was recorded upon increasing the HA amount. The sigmoidal plot profile of the ζ-potential on *r*HA

allows for the extrapolation of *r*HA at which the charge ratio is equal to zero, yielding ~ 0.45, hence in nice agreement with theoretical calculations (see above).

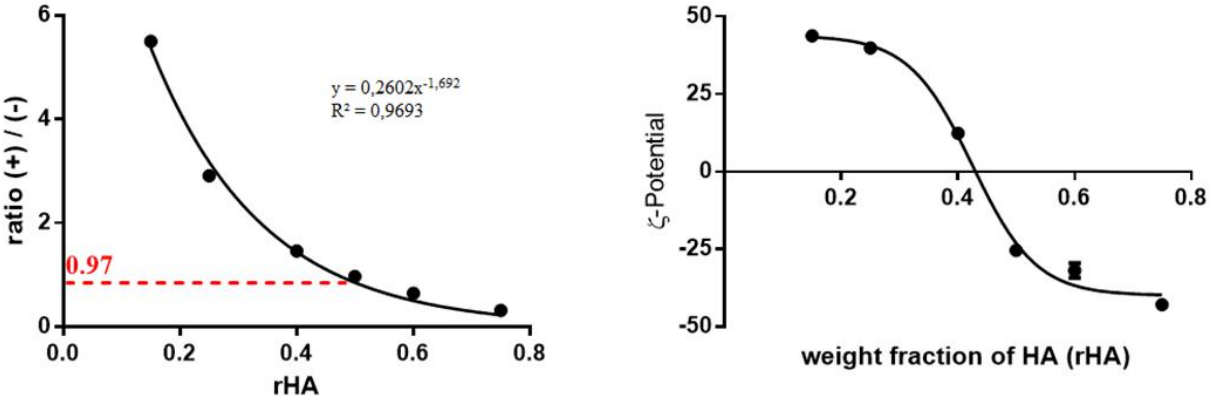

Figure 14: A) Theoretical evaluation of the ratio between positive and negative charges of the binary solutions with respect to *r*HA. Calculations were performed assuming that at pH 4.5 both polymers were fully charged B) ζ-potential analyses of the surface charge of formulation prepared at pH 4.5, dropping of HA into CTL and without supporting salts. Results are reported as means (± SD, *n* = 3).

Finally, the impact of HA molecular weight on complex coacervation was herein investigated. An increment of turbidity was observed whatever HA (HA310 or HA500) used for coacervates preparation (Figures 15 and 16). The modality of mixing had negligible effect on *T*, since transmittance remained below 40% for all the formulations investigated, confirming the associative phase separation. The presence of small amounts of precipitates was also found for binary mixtures using HA310 and HA570, in line with that previously reported. Hence, one can conclude that only in the case of *r*HA 0.15 and dropping of HA into CTL60 the formation of insoluble aggregates may be prevented.

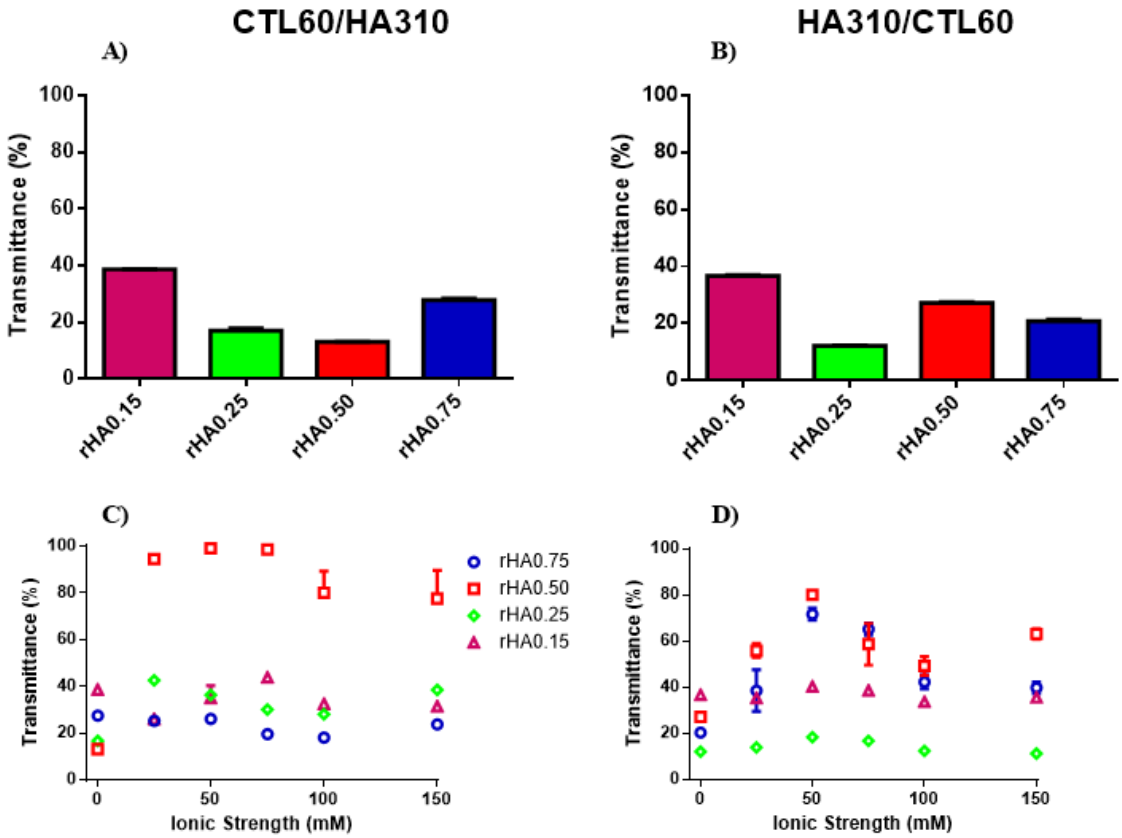

Figure 15: Panel representing the analyses of the Transmittance of the formulations prepared using CTL60 and HA310. Influence of pH (A and B) and ionic strength (C and D) on the Transmittance of the binary mixture solutions of HA and CTL prepared at different *r*HA. A) and C) Formulations prepared by dropping CTL60 solution into HA310 solution. B) and D) Formulations prepared by dropping HA310 solution into CTL60 solution. Results are reported as means (± SD, *n* = 3).

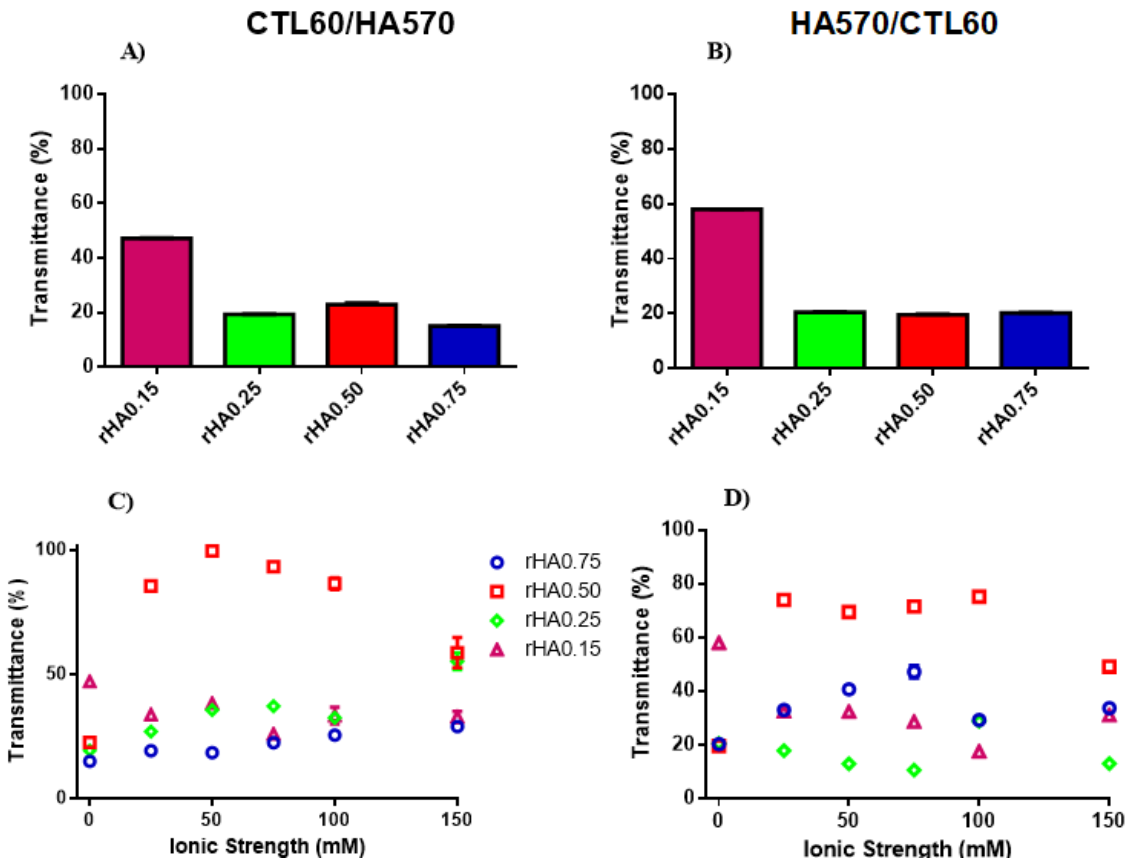

Figure 16: Panel representing the analyses of the Transmittance of the formulations prepared using CTL60 and HA570. Influence of pH (A and B) and ionic strength (C and D) on the Transmittance of the binary mixture solutions of HA and CTL prepared at different *r*HA. A) and C) Formulations prepared by dropping CTL60 solution into HA570 solution. B) and D) Formulations prepared by dropping HA570 solution into CTL60 solution. Results are reported as mean (± SD, *n* = 3).

DLS technique was used to prove the presence of coacervates in the solutions prepared at pH 4.5 and to deeply investigate the influence of HA molecular weight and *r*HA on the size, polydispersity and surface charge.

We started by analyzing the simplest system in pure deionized water. A comparison of the size and volume distribution profiles of three formulations prepared at the same *r*HA but different HA molecular weight is reported in Figure 17. Coacervates prepared with HA90 and *r*HA of 0.75 displayed good homogeneity (PDI = 0.28 ± 0.02), in line with what reported in literature for biopolymer-based nanoparticles [33,84], whereas a more heterogeneous distribution was noticed for systems prepared using HA310 (PDI 0.56 ± 0.05) and HA570 (PDI 0.55 ± 0.21). Two peaks with weak intensity were detected for formulations using HA310, ascribed to the presence of very small

scatters (peak around 70 nm) or aggregates (> 1000 nm). More variable results were obtained using HA570. Our findings suggest that, by increasing HA molecular weight, the size and polydispersity of coacervates tend to increase, thus diverging from a homogeneous ensemble of colloids. It can be hypothesized that CTL60 is more prone to accommodate HA90 due to very different molecular weight between polysaccharides, *i.e.* 910 000 vs. 90 000, favoring associative phenomena. In this view, HA90 may be envisaged as a cross-linker for CTL60. A further consideration stems from the dimensional shift of the main intensity peak toward larger values by increasing HA molecular weight (Figure 17A), confirming again the role played by the macromolecule size in modulating the final dimension of caocervates. In this view, higher molecular weight HAs lead to steric hindrance, thereby enabling the formation of heterogeneous and larger aggregates rather than homogeneous spherical coacervates. These findings are in line with what reported in literature for colloidal coacervates chitosan/tripolyphosphate (TPP)-based [85] [86], where lower molecular weight chitosans were found being the best choice for synthetizing monodispersed particles [87][88]. The comparison of the intensity and the volume size distributions highlight that the curves match almost perfectly in the case of coacervates with HA90, whereas deviation from linearity together with the presence of multiple peaks are evidenced when HA310 and HA570 were used (Figure 17B). Again, it has to be recalled the negative role played by higher molecular weight HAs for the final homogeneity of the system.

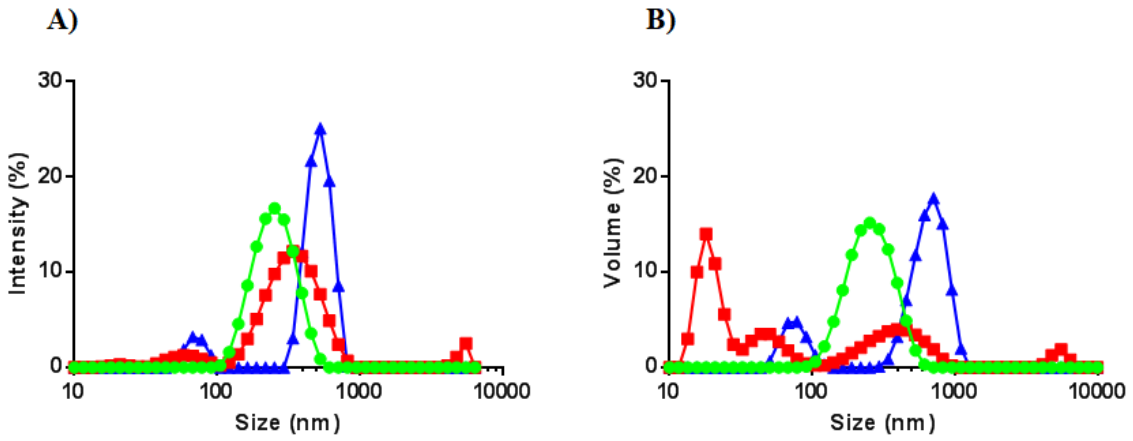

Figure 17: DLS analyses of the influence of the three different molecular weight HAs on the formulation prepared at pH 4.5, *r*HA 0.75 and by dropping HA into CTL60. A) Size distribution and B) Volume distribution. HA90/CTL60 spectrum is reported in green, HA310/CTL60 spectrum is reported in red and HA570/CTL60 spectrum is reported in blue.

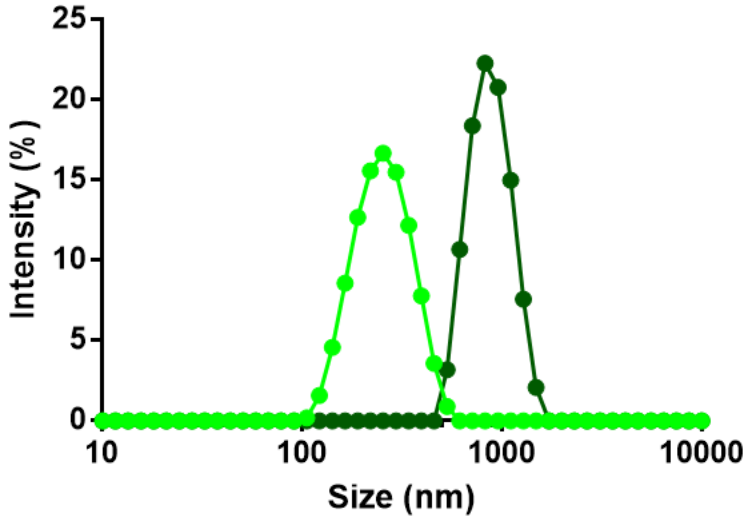

Figure 18: DlS analysis of the influence of the weight fraction of HA (*r*HA) on the coacervates formation. Coacervates were both prepared by dropping HA90 into CTL60, pH 4.5 and negligible ionic strength. Light green peak (*r*HA0.75), dark green peak (*r*HA0.25)

DLS analyses displayed also the influence of *r*HA on the size of coacervates prepared with HA90 (Table 3). The size of coacervates passed from around 200 nm (*r*HA 0.75) to almost 1 μm (*r*HA0.25) by increasing the content of CTL, whereas the PDI of the system remain the same. Such difference is related to the increase of CTL content; its higher molecular weight, with respect to HA90, leads to the formation of larger coacervates.

Sample	Size (nm)	PDI
HA90/CTL60 *r*HA0.75	255 ± 6	0.28 ± 0.02
HA310/CTL60 *r*HA0.75	295 ± 5	0.56 ± 0.05
HA570/CTL60 *r*HA0.75	487 ± 83	0.55 ± 0.21
HA90/CTL60 *r*HA0.25	978 ± 3	0.27 ± 0.02

Table 3: Comparison of size and PDI of coacervates prepared with HAs at different molecular weight and weight fraction (*r*HA).

To recapitulate, the present results demonstrate that variables as pH, ionic strength, weight ratio between the polysaccharides and macromolecular dimensions are pivotal factors in determining positive complex coacervation outcomes with good control of the whole process.

CHAPTER 2: Preparation and characterization of HA/CTL coacervates

3.2.1 Aim of the work

This second chapter deeply analyze the features of complex coacervates. In particular, one formulation, namely HA90/CTL60 with *r*HA0.25, was selected as the best candidate for coacervates preparation. The stability in physiological ionic strength, pH and temperature was investigated. Moreover the storage stability of the coacervates for commercial purposes was assessed by freezing-drying of the coacervates solution. The possibility to efficiently encapsulate and release a model payload was explored, giving the final aim of preparing a system for drug release. Biological evaluation of the influence of coacervates both on neutrophils and on osteoblast cell line was carried on.

3.2.2 Materials and Methods

3.2.2.1 Materials

HEPES buffer, acetic acid, sodium acetate, Percoll, 2-(N-morpholino)ethanesulfonic acid (MES), bovine serum albumin (BSA, Cohn fraction V, ≥96% cell culture-tested), dihydrorhodamine 123 (DHR), horseradish peroxidase (HRP), fluoresceinamine isomer I, dexamethasone, type VI, fibrinogen (FBG) from human plasma, Alamar Blue, and sodium hydroxide were purchased from Sigma-Aldrich Chemical Co. Hydrochloric acid was purchased from Carlo Erba (Milano, Italy). Deionized Milli-Q water was used throughout. All solutions used in the biological assays were prepared in endotoxin-free water or saline (0.9% w/v NaCl) for clinical use. DMEM High Glucose, Trypsin-EDTA 1X, Penicillini-streptomycin were purchased by Euroclone s.p.a (Milano, Italy)

3.2.2.2 Characterization of coacervates

Dynamic Light Scattering (DLS) measurements were performed using a Zetasizer Nano ZS system (Malvern Instruments, Inc., Southborough, MA), in order to evaluate the intensity of 173° scattered light (Derived Count Rate - kilocounts per second, kcps), the average hydrodynamic diameter and the polydispersity index (PDI) of the coacervates prepared in the presence of NaCl. Coacervates solutions were diluted 1:10 v/v in the same buffer in which the soluzion are prepared (pH 4.5) and DLS measurements were performed at 25 °C, analyzing each sample in triplicate. The morphology and the size of HA/CTL coacervates were examined by Transmission Electron Microscopy (TEM). 10 μL of colloids were placed on a carbon film 300 mesh copper grid and air-dried. The sample was stained with 10 μL of a 0.1% w/v uranyl acetate solution for 2 min at room temperature before acquiring images by means of Philips EM 208 microscope, using an accelerating voltage of 100 kV.

3.2.2.3 Dissolution stability as a function of pH and time

DLS analyses were performed in order to check the stability of coacervates at different pH values. Specifically, coacervates were synthetized at pH 4.5 (see paragraph 3.1.2.3) and pH increased by addition of NaOH 0.1 M under gently stirring. The transmittance, *T*, and the light scattered at 173° (*i.e.* derived count rate) were analyzed for solutions at selected pH values. Coacervates stability was also evaluated by incubating the samples at 37 °C. DLS measurements were performed immediately after the synthesis of coacervates and after 1, 3, 7, 14 and 21 days of incubation, respectively.

3.2.2.4 Effect of freeze-drying on coacervate stability

The stability of coacervates after freeze-drying was evaluated both in the presence and absence of trehalose as cryoprotectant. Trehalose was solubilized in deionized water (10% w/v final

concentration). Coacervates were diluted 1:2 v/v with cryoprotectant, and the resulting solutions were further diluted 1:5 v/v in deionized water prior DLS analyses. Samples in the presence/absence of cryoprotectant were placed in 1.5 mL tubes and freeze-dried overnight. Resulting formulations were then suspended in the same volume of buffer, vortexed and analyzed in triplicate by DLS after dilution 1:5 v/v in deionized water.

3.2.2.5 Encapsulation of a model molecule

Fluoresceinamine isomer I and dexamethasone were selected as model-payloads to determine the encapsulation efficiency and drug loading capacity of the selected formulation. The former molecule was solubilized in methanol (1 mg/mL final concentration) and used to prepare serial dilutions using acetate buffer 10 mM and NaCl 150 mM as the solvent. The linear range of fluorescence intensity as a function of concentration (buffer without fluorophore as blank) was recorded using a BMG LABTECH 96 spectrofluorometer, with λex = 485 nm and λem = 520 nm. The fluorophore was added at a final concentration of 2 µg/mL to 1.5 mL of CTL solutions. In the case of dexamethasone, the final concentration was 20 µg/mL; the absorbance was recorded at λ = 241 nm using a Ultrospec 2100 pro (Bioscience, England). Molecule-loaded coacervates were left 5 min under stirring to homogeneously distribute the payload. Finally, 500 µL of HA were added dropwise and the mixtures stirred for 15 min. 500 µL of the particles solution were placed in 1.5 mL tubes and centrifuged at 9 000g for 1 h. After centrifugation, the supernatants were collected and analyzed. The supernatant of coacervates prepared without payload was used as blank. Calibration curves were used to determine the molecules concentration in the supernatant. Encapsulation efficiency (%) was determined according to eq 4:

$$EE = \frac{C_x - C_i}{C_i} \, x \, 100 \qquad (4)$$

where C_i corresponds to the initial concentration of the payload, C_x is the payload concentration in the supernatant after sample centrifugation. Loading capacity (expressed as w/w ratio) was determined as eq 5:

$$LC = \frac{w_t - w_x}{w_p} \qquad (5)$$

where w_t corresponds to the total mass of the encapsulated molecule, w_x is the mass recovered from the supernatant, and w_p is the mass of coacervates. [89] Payload-loaded samples were also analyzed by DLS to evaluate their hydrodynamic diameter and PDI.

3.2.2.6 Release experiments

The leakage of dexamethasone from HA/CTL47 coacervates was measured in AcOH/AcNa buffer 10 mM as final concentration (pH 4.5, NaCl = 150 mM) at 37 °C. Dexamethasone was encapsulated at a final concentration of 20 μg/ mL, and resulting coacervate dispersions were sealed in a dialysis tube (Sigma-Aldrich, cutoff 12 kDa) and placed in 2 mL of the same buffer under shaking conditions. The dialysis solution was collected and replaced with fresh buffer after each time investigated. The amount of dexamethasone was quantified as indicated in paragraph 3.2.2.5. The release of dexamethasone from HA/CTL47 coacervates was monitored up to 4 h, and results are reported as the percentage of cumulative release over time.

3.2.2.7 Isolation of human neutrophils

Venous blood was collected from healthy volunteers after obtaining written informed consent, with the approval of the Institutional Ethical Committee. Neutrophils were isolated by a discontinuous Percoll gradient centrifugation as previously described, [90] and suspended in PBS solution, pH 7.4, containing 5 mM glucose and 0.2% BSA. Immediately before use, cell suspensions were washed in MES-buffered saline solution (MBS) containing 140 mM NaCl, 5 mM

KCl, 5 mM glucose, 10 mM MES (pH 6.0), and 0.2% BSA (MBS-BSA), and suspended in the same medium.

3.2.2.8 Preparation of FBG-coated surfaces

Flat-bottom poly(styrene) wells (F16 MaxiSorp Nunc-Immuno Modules or F16 Black MaxiSorp Fluoronunc Cert, Thermo Fisher Scientific, Roskilde, Denmark) were coated with FBG as described elsewhere. [91] Briefly, 50 μL of a FBG solution (400 μg/mL in PBS) were placed in each well, and the plate was left at 37 °C for 2 h in a humidified chamber. Prior to use, the wells were rinsed three times with PBS.

3.2.2.9 Evaluation of H_2O_2 production

H_2O_2 generation was assessed using DHR. Neutrophils (1.25 × 106 cells/mL in MBS-BSA) were loaded with 40 μM DHR for 30 min at 37 °C in a shaking water bath, in the dark. Five to ten minutes before starting the assay, the cell suspension was supplemented with 1 mM CaCl2 and 1 mM MgCl2. Then, 60 μL aliquots of this suspension were dispensed into FBG-coated black wells containing the HA/CTL coacervates (50 - 150 μg/mL final concentration) or the same volume of acetate buffer solution, and HRP (1 μg/mL final concentration), in a total volume of 0.15 mL MBS-BSA supplemented with 1 mM CaCl2 and 1 mM MgCl2 (Ca2+/Mg2+ MBS-BSA). The plate was incubated at 37 °C in the dark and at the desired times readings were taken with a microplate fluorescence reader (Tecan Infinite F200; Tecan Austria GmbH, Grodig, Austria) at 485 nm (λ ex) and 535 nm (λ em). H_2O_2-independent oxidation of DHR was measured in wells containing DHR loaded neutrophils pretreated for 10 min with the NADPH-oxidase inhibitor DPI (5 μM final concentration), and the fluorescence values registered at each incubation time were used as a baseline and subtracted from the actual experimental ones.

3.2.2.10 Measurement of neutrophil adhesion

The number of neutrophils adherent to FBG was assessed by quantifying myeloperoxidase activity as described in Reference. [90] Adhesion tests were conducted in FBG-coated transparent wells to monitor cell morphology by light microscopy, and were run in parallel and in the same experimental conditions of those used to evaluate H_2O_2 production, except for the omission of DHR and HRP.

3.2.2.11 Assessment of cells viability

To assess the biocompatibility of complex coacervates at pH 7.4, viability studies on MG-63 cell line were conducted. Coacervates were prepared using the EDC-NHS chemistry to stabilize them at physiological pH. MG-63 cells were seeded in a 96 well plate at a final concentration of $5x10^3$ cells/well and treated with different amount of coacervates, namely 150 μg/mL, 100 μg/mL and 50 μg/mL. Cells cultured in DMEM without coacervates or in DMEM with hydrogen peroxide were used as positive and negative viability control. Cell viability was verified after 4 hours, 1 and 3 days. 4 replicates were analyzed for each condition.

3.2.2.11 Statistical Analysis

Statistical analysis was performed with Student's t-test, using GraphPad Prism 5.0 (GraphPad Software, San Diego, CA). p-values less than 0.05 were considered statistically significant.

3.2.3 Results and discussion

Previous analyses of Transmittance and DLS pointed out the formation of complex coacervates fostered by the electrostatic interaction between CTL60 and HA90. DLS analyses confirmed the presence of spherical particles in solution. Moreover, by comparing formulation of HA90/CTL60 prepared with *r*HA0.75 and *r*HA0.25 it was shed light on the influence of the ratio of the two polymer on the size of the coacervates. We decided to move forward with further analyses using the formulation HA90/CTL60 with *r*HA0.25. Even though this formulation displayed a higher particle size with respect to the formulation HA90/CTL60 *r*HA0.75, the Transmittance values underlined its great stability through all the range of ionic strengths investigated. Such stability is of primary importance, giving the final aim of using this system for biomedical purposes.

By comparing the Transmittance values of the HA90/CTL60 formulation with *r*HA0.25 at negligible ionic strength and in the presence of 150 mM of ionic strength it is evident an increased of the turbidity of the system, without precipitates in the solution (Figure 19A). This result joints other works on coacervation demonstrating that the increase of turbidity following salt addition - up to some extent - is a typical behavior of nonstoichiometric polyelectrolyte complexes. [92,93] To give further insights into the complex coacervation between hyaluronan and CTL60, dynamic light scattering analyses were carried out on the same samples (Figure 19B). The size distributions by intensity indicate a monodispersity curve profile for coacervates synthesized both without supporting salt and in the presence of NaCl 150 mM, thus suggesting that a homogeneous ensemble of (spherical) scatters was present. Strikingly, a significant shift toward smaller size values was noticed in the latter case, with the hydrodynamic diameter passing from 980 ± 90 nm to 454 ± 29 nm. These results are in line with what was found by Kayitmazer and co-workers. [83] Specifically, in the quoted paper the authors identified a decrement of colloids dimension following the increase of the ionic strength up to 0.15 M; beyond this value, an abrupt coacervates size increase was detected. Though the latter behavior may be reasonably interpreted in terms of large clusters

formation due to the vanishing of electrostatic repulsions among smaller colloids, the reduction of coacervates dimensions in the presence of 150 mM NaCl should conversely take into account the simple role played by the ionic strength in reducing the (overall) hydrodynamic diameter of both the macromolecules. It is therefore expected that CTL and HA would assemble in smaller, more compact, and homogeneous coacervates. As expected, the homogeneity of the system increased in the presence of the supporting salt, showing a significant decrease of the polydispersity index (PDI) from 0.27 ± 0.02 for the coacervates fabricated without supporting salt to 0.14 ± 0.03 for those formed in NaCl 150 mM.

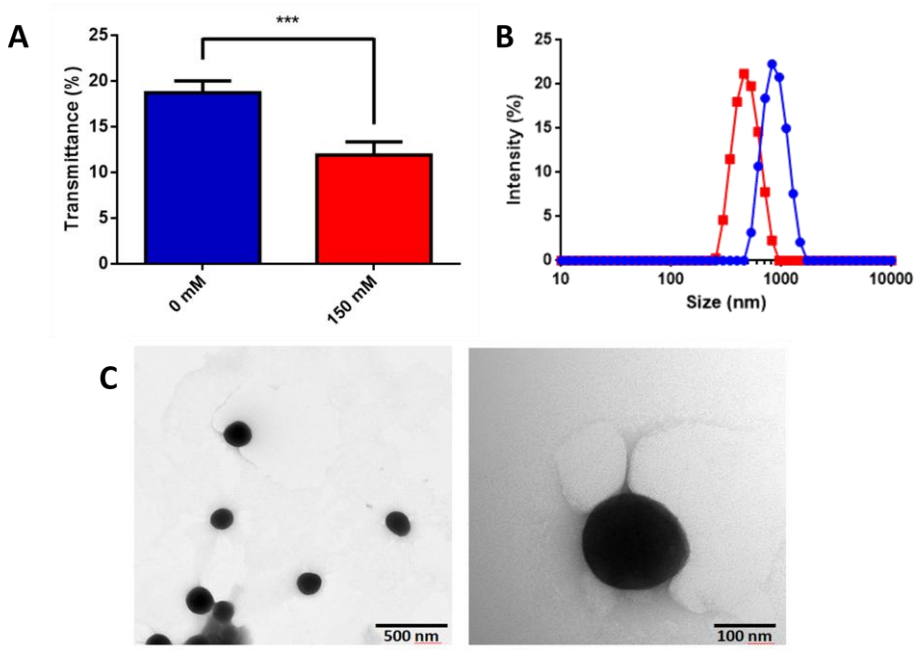

Figure 19: (A) Influence of the ionic strength on the transmittance of coacervate solutions prepared at pH 4.5, dropping hyaluronan into CTL60 solutions. Results are reported as mean (±SD, n = 5). Statistical analysis: coacervates formed without NaCl vs coacervates formed in the presence of NaCl 150 mM: Student's t-test: ***, p < 0.001. (B) DLS investigation on the influence of ionic strength on coacervates formation. Size distribution of formulations prepared without supporting salt (blue) and with NaCl 150 mM (red). (C) TEM images of coacervates synthesized in the presence of NaCl 150 mM and subsequently diluted 1:100 v/v in deionized water to acquire images.

Sample-case transmission electron microscopy (TEM) images of coacervates synthesized in the presence of NaCl 150 mM corroborated the good homogeneity and the spherical shape of colloids (Figure 19C). Finally, it is of primary importance to underline that CTL60 and HA not only were able to form spherical and homogeneous coacervates in the presence of high salt content

(resembling the physiological ionic strength), but even that the formation of coacervates occurred immediately after the polymer dropping, without any phase separation lag or equilibration times. These results highlight an important difference between simple coacervation (*i.e.*, involving one macromolecule) and complex coacervation (involving two or more macromolecules): indeed, in several studies, the ionotropic gelation of chitosan and its derivative CTL using tripolyphosphate (TPP) as cross-linker is drastically hampered by elevated NaCl (*i.e.*, 150 mM) and low TPP amounts, [94] [61] mostly in the first stage of macromolecular assembly. Therefore, the use of hyaluronan - presently envisaged as a low MW "cross-linker" for CTL - in fostering the formation of complex coacervates in physiological osmolarity is more effective than the multivalent anion TPP.

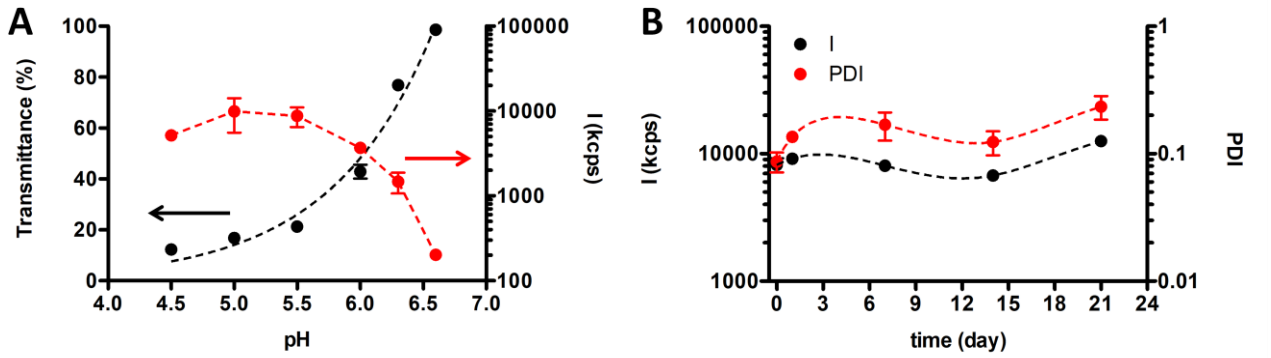

Figure 20: (A) Dissolution stability of HA/CTL60 coacervates as a function of pH: transmittance (black dots) and intensity of 173° scattered light (red dots) recorded from DLS measurements: dashed lines are drawn to guide the eye. (B) Dissolution stability of HA/CTL60 coacervates as a function of time. 173° scattered light (black dots) and polydispersity index?PDI?(red dots). Coacervates were kept at 37 °C for 21 days and DLS measurements performed at selected timepoints; dashed lines are drawn to guide the eye. All results are reported as mean (±SD, n = 3).

The stability of coacervates as a function of pH and time was studied thereafter. Transmittance studies pointed at constant values for *T* (below 40%) up to pH 5.5; beyond that, an increase of *T* of about 20% marked the initial instability of the system (Figure 20A). Moreover, the formation of visible aggregates was detected above pH 6.3. The complete dissolution of coacervates was noticed in the high pH range, as noticed by *T* values reaching those of disentangled polymers.

The opposite trend of the scattering intensity data at 173° reported in the same figure validated the instability of the system at pH ≥ 6. Specifically, a sudden decrement of scattering intensity paralleled by an increase of *T* was observed at pH > 6, thus pointing at the onset of coacervates dissolution. The polydispersity index computed from DLS supported the transition from almost homogeneous colloids (PDI = 0.14 ± 0.03) to aggregates with variable dimensions (PDI = 0.48 ± 0.20). It can be concluded that coacervates largely dissolve in a range of pH 6.0−6.3, even if the presence of residual chain aggregates cannot be excluded given the residual scattering intensity.

Coacervates stability was subsequently studied as a function of time at 37 °C and pH = 4.5. An almost constant profile of scattering intensity was observed up to 14 days of incubation (Figure 20B). A slight increase of both derived count rate and PDI occurred after 3 weeks at 37 °C, indicating a reasonable swelling or partial aggregation of the coacervates. Size distribution curves were almost comparable after 21 days of incubation (data not shown); moreover, the absence of visible aggregates indicated that coacervates remained stable throughout the experiment. This result indicated a clear difference with the CTL/ TPP case, indicating that the use of hyaluronan provides an additional benefit with respect to TPP. [61] Indeed, the replacement of the multivalent anion with low molecular weight hyaluronan produced stable particles at physiological temperature.

To further improve the stability of coacervates against dissolution at slightly acidic pH values tending to neutrality, the hypothesis to use CTL samples with different fraction of lactose-modified units (F_L) was considered. CTL samples having different F_L values present different fraction of both primary and secondary amines, meaning that they would be differently influenced by pH variation. Indeed, the calculated pKa values for primary and secondary amines were 6.69 and 5.87, respectively. It is therefore expected that CTL samples endowed with a lower degree of substitution would better withstand the pH increase from 5.5 to 6.5. Hence, a second CTL sample with F_L = 0.47, CTL47, was used to form coacervates. The comparison of the size intensity distributions for the two types of formulations is reported in Figure 21A. The two different

formulations peak at almost identical size (HA/ CTL60 = 454 ± 29 nm, HA/CTL47 = 461 ± 67 nm) and show a very similar (Gaussian-like) distribution. This finding clearly indicates that a 13% difference in the values of lactitol branching and the slight discrepancy in terms of CTL molecular weight did not greatly influence the formation and the homogeneity of coacervates. At variance, it seems that the almost identical charge [−]/[+] ratio - *i.e.* 0.24 and 0.26 in the case of coacervates prepared with CTL47 and CTL60, respectively - contributes to such a similar behavior. The pH profile of the turbidity of the HA/CTL47 system paralleled that of HA/CTL60, transmittance, *T*, increasing with increasing pH. However, for pH = 6.0 and beyond, the *T* values of the systems containing CTL47 showed a progressively lower value of *T*, up to pH 6.3, for which T = 39.4 ± 0.4 for F_L = 0.47 and *T* = 76.9 ± 1.3 for CTL with F_L = 0.60. This finding was also supported by DLS analysis, where, although the scattering intensity decreased in a similar fashion, the data of the systems based on CTL47 always showed intensity values larger than those of the CTL60 systems (Figure 21C). Hence, the stability against dissolution can be improved by decreasing the fraction of lactose-modified units from 0.60 to 0.47. By further increasing pH, it was found that coacervates made of F_L = 0.47 CTL remained stable at pH 6.6 for approximately 40 min, whereas a complete dissolution of the system occurred subsequently, suggesting that a kinetically controlled effect is also involved in the dissolution of coacervates. Finally, the time-stability at 37 °C and pH = 4.5 was verified up to 21 days for the latter formulation, showing a very similar behavior if compared with F_L = 0.60 counterparts (data not shown).

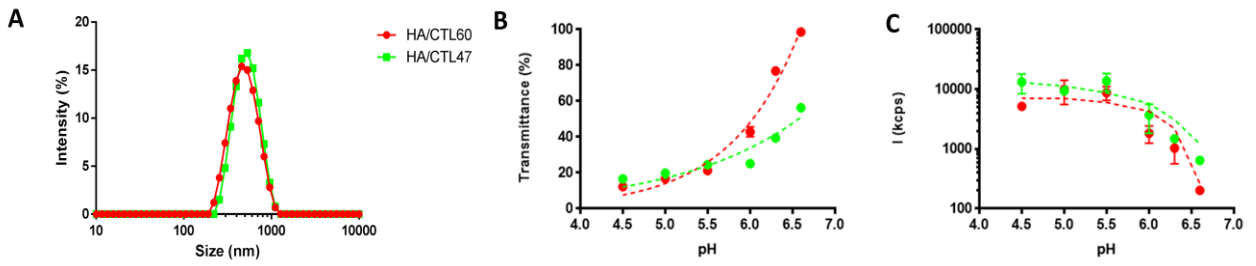

Figure 21: (A) DLS size distribution curves of coacervates synthesized with different CTL samples. All formulations were prepared at pH 4.5, AcOH/AcNa buffer 10 mM and NaCl = 150 mM. Dissolution stability as a function of pH: (B) transmittance and (C) DLS analyses. Color legend: HA/CTL60 (red dots) and HA/CTL47 (green dots). Results are reported as mean (±SD, n = 3). Dashed lines are drawn to guide the eye.

The possibility to freeze-dry suspensions of coacervates for long storage purposes was investigated. DLS results obtained on both freshly prepared and dried coacervates are reported in Figure 22. Both formulations, i.e. with F_L = 0.60 or F_L = 0.47, were freeze-dried in the presence or absence of trehalose as cryoprotectant. [95] The results in Figure 22A indicate that freeze-drying without trehalose brought about a massive and uncontrolled aggregation of particles. The presence of trehalose was beneficial for the impact of the freeze-drying process for both F_L values. The values of both PDI and intensity showed a net benefit using trehalose as a cryoprotectant. In particular, coacervates based on CTL47 and containing trehalose showed both PDI and intensity values after freeze-drying practically equal to the corresponding values before freeze-drying. DLS analyses clearly proved that the use of trehalose as cryoprotectant is necessary for the storage of HA/CTL coacervates. The present results differ from what was reported in our previous contribution for simple coacervation systems based on CTL60 and TPP, where the presence of trehalose resulted as detrimental for the freeze-drying process. [61] This difference could stem from a different alignment of the polycationic (CTL) part with the polyanionic counterpart in the case of TPP with respect to HA. Possibly, in the former case, the much shorter dimension of the cross-linking agent could leave a large number of lactitol side-chains still free to interact with water ensuring an antifreezing effect. The observation that, in such conditions, the addition of trehalose is detrimental for the coacervate integrity might suggest a sort of “competition” between the lactitol side-chains and the added trehalose with respect to the ability of interfering with water-freezing. At variance, in the latter case the longer stretch of the polymeric arrangement could immobilize longer lactitol-containing sequences of CTL, thus canceling their potential of interference with water-ordering (and crystallization) upon freeze-drying. As a result, the addition of trehalose could act as a restoring agent of the anti-freezing potential of the intact CTL moiety. The effect of the lactitol content on both PDI and dimension of coacervates was of interest. Whereas in the case of CTL47 the proposed polycation/polyanion alignment seemed to cancel the lactitol effect on water crystallization in the absence of trehalose, the addition of the latter seemed to be able to restore the

antifreeze effect. At variance, in the case of CTL60 the larger amount of lactitol partially counterbalanced the positive effect of the addition of trehalose as suggested by the fact that with trehalose neither PDI nor dimensions reattain the values of the "normal" condition, providing an indirect support to the hypothesis of a "competition" between lactitol and trehalose in their antifreeze ability.

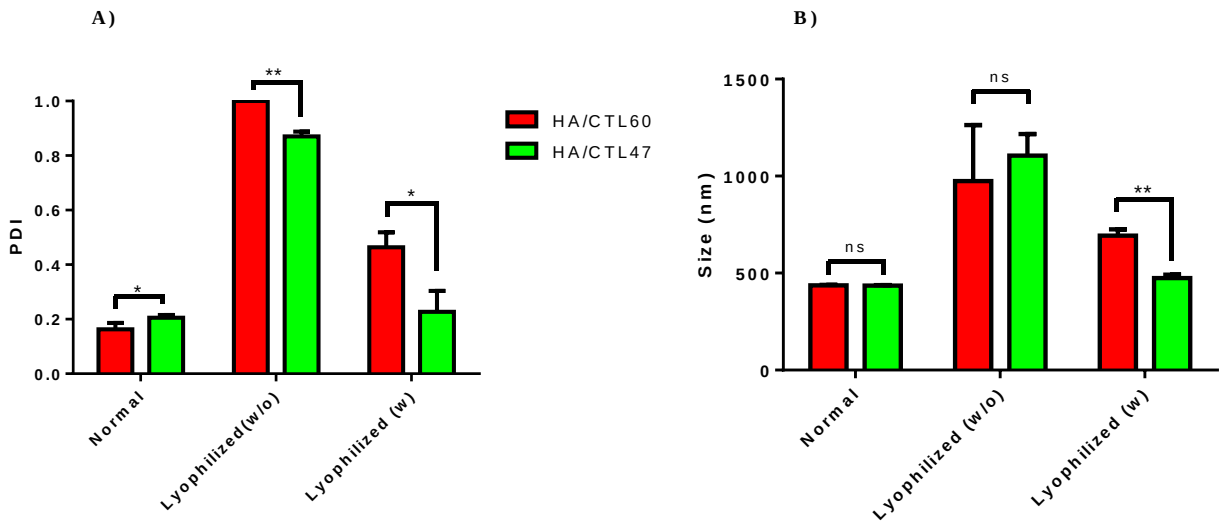

Figure 22: Storage stability of coacervates. PDI (A) and average hydrodynamic diameter (B). Coacervates were analyzed before (Normal) and after the freeze-drying process in the presence (Lyophilized-w) or absence (Lyophilized-w/o) of trehalose. Color legend: HA/CTL60 (red), HA/ CTL47 (green). Results are reported as mean (±SD, n = 3). Statistical analysis: HA/CTL60 vs HA/CTL47. Student's t-test: *, p < 0.05; **, p < 0.01; NS, not significan.

The ability of coacervates to encapsulate proper payloads was investigated to consider them as potential drug delivery systems. Fluoresceinamine isomer I was used at first as model molecule and the synthesis of coacervates was performed as described in paragraph 3.2.2.5. CTL samples at two different F_L values formed coacervates with similar dimensions and homogeneity even when hosted the payload, as detected by DLS analysis (data not shown). The two formulations showed an identical ability to encapsulate fluoresceinamine isomer I (Table 4). The calculated loading capacity was 0.65 µg payload/mg carrier, with an encapsulation efficiency around 96%, which is in line with

similar systems. [33] [34] The encapsulation efficiency and drug loading for HA/CTL47 coacervates were verified also using dexamethasone as payload, yielding 56 ± 1% and 3.74 ± 0.07 µg payload/mg carrier, respectively. In vitro release experiments were undertaken to study the leakage of dexamethasone from HA/CTL47 coacervates, and results are reported in Figure 23. The release profile of the payload over time was almost constant up to 1 h of incubation, with around 80% of total drug released. After longer incubation time, the release profile tended to reach a plateau with almost total dexamethasone released during 4 h of incubation. Overall, our findings demonstrated that HA/CTL47 coacervates were able to gradually release the selected payload in the early stages of incubation.

Payload	Sample	Encapsulation Efficiency (%)	Loading Capacity (µg/mg)
Fluoresceinamine	HA/CTL60	97 ± 6	0.65 ± 0.04
	HA/CTL47	98 ± 5	0.65 ± 0.03
Dexamethasone	HA/CTL47	56 ± 1	3.74 ± 0.07

Table 4: Encapsulation Efficiency and Loading Capacity of Coacervates Prepared with Hyaluronan and CTL at Different Fractions of Lactose-Modified Units (FL). Conditions: synthesis at pH 4.5, NaCl = 150 mM, room temperature.

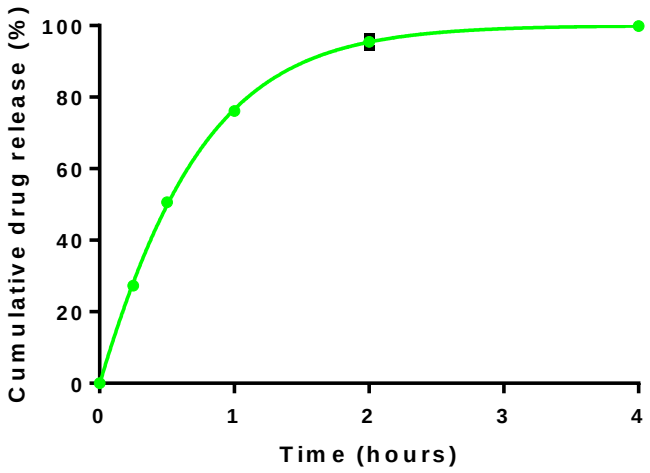

Figure 23: Cumulative release of dexamethasone from HA/CTL47 coacervates. Conditions: AcOH/AcNa buffer 10 mM, NaCl = 150 mM, pH 4.5, T =37 °C. The results are reported as mean (±SD, n = 3). Dashed line is drawn to guide the eye.

Both HA/CTL60 and HA/CTL47 systems resulted to be unstable at neutral pH. However, the HA/CTL47 system proved to be reasonably stable at acidic pH, namely at pH 6. Extracellular acidosis is a condition commonly associated with inflammatory processes, where extracellular pH values as low as 6.1 have been documented. [96] [97] Moreover, acidic pH values were found in the cancer microenvironment. [98] pH-dependent features of chitosan/hyaluronic acid-based nanoparticles have been a matter of investigation by other authors. [33][99] In view of its potential use in vivo as a drug carrier, the HA/CTL47 system was selected to perform in vitro experiments in acidic pH conditions, namely pH 6.0. We decided to evaluate the effect of CTL47-based coacervates on neutrophils, which represent a key first-line defense of the immune system. Specifically, the possibility that coacervates could modulate the generation of H_2O_2 and/or the adhesion of neutrophils to FBG was tested. Figure 24A shows that coacervates, at the tested concentrations, had only a minor stimulatory effect on the basal production of H_2O_2 by human neutrophils at pH 6.0. However, the coacervates elicited a marked increase in the number of cells adherent to FBG (Figure 24B), which was accompanied by an exacerbation of the elongated morphology exhibited by neutrophils at this pH value. The expected increase in cell adherence stimulated by HA/CTL47 prompted us to replot the data obtained in the DHR assay and normalize them on the basis of cell adhesion (Figure 24C). Surprisingly, the new plotting unraveled that the increased number of adhered cells, as a whole, produced a lower amount of H_2O_2 than control neutrophils incubated in the absence of the coacervates. Such a reduction of H_2O_2 generation could be explained by a HA/CTL47-mediated scavenging effect, since both HA and chitosan, from which CTL is obtained, have been shown to be efficient ROS scavengers. [34] [96] Moreover, we have recently demonstrated that chitosan/HA nanoparticles are capable of scavenging O_2^-/H_2O_2 released by neutrophils. [30] Taking the cue from some literature data, additional hypotheses to explain the effect of HA/CTL47 on adherence and/or ROS production could be proposed. The former one calls in the possibility that the interaction between neutrophils and the coacervates, involving as-yet unidentified surface receptor(s), somehow enhances the affinity of β2 integrins, thereby improving

neutrophil adherence to FBG. [100] Such an increased adherence would then trigger intracellular signals which downregulate ROS production, similarly to what has been described to occur after the interaction of αvβ3 integrin with fibronectin. [101] As a latter alternative, the contact of HA/CTL47 with neutrophils could signal for an improved activity of ROS degradative enzymes, such as catalase and superoxide dismutase, thus resembling the quercetin-mediated effect that has been documented in a model of neuroinflammation using a human neuroblastoma cell line. [102] Clearly, specific investigation is additionally required to clarify this interesting point.

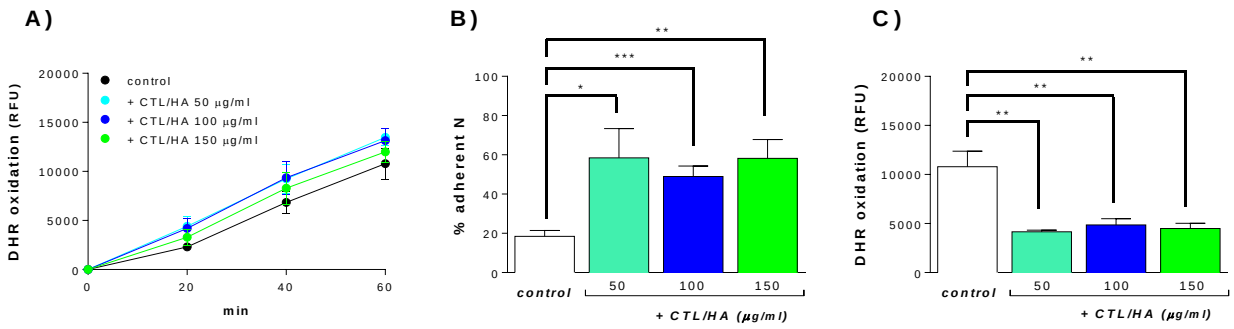

Figure 24: Effect of HA/CTL47 coacervates on neutrophil H2O2 production and adhesion to fibrinogen (FBG). The coacervates were prepared at pH 4.5. The pH was then raised to 6.0 before performing biological experiments. (A) Time-course of H2O2 generation. Dihydrorhodamine 123 (DHR)-loaded neutrophils (suspended in Ca2+/Mg2+ MBS-BSA) were incubated at 37 °C in the absence or presence of coacervates, in FBG-coated wells containing horseradish peroxidase (HRP). H2O2 production was evaluated by fluorometric measurement of oxidized DHR. Data are means (±SE) of two triplicate experiments. (B) Adhesion of neutrophils to FBG. Adhesion was quantified after 60 min of incubation by measuring myeloperoxidase activity as detailed in the Materials and Methods. Data are means (±SE) of two triplicate experiments. (C) H2O2 production at 60 min of incubation. Results reported in (A) have been normalized for the number of adherent cells (B). Statistical analysis: coacervates-treated neutrophils vs control neutrophils. Student's t-test: *, $p < 0.05$; **, $p < 0.01$; ***, $p < 0.001$.

HA90/CTL47 coacervates displayed an improved pH stability with respect to those prepared using CTL60, but unfortunately they tended to dissolve if the pH was raised toward neutrality due to loss of positive charges on CTL. Given the final application of complex coacervates for biomedical purposes, we applied the EDC-NHS coupling to stabilize them. EDC [1-Ethyl-3-(3-dimethylaminopropyl)carbodiimide] is already used in the TE field as chemical cross-linker for biomaterials stabilization. [103] As a matter of fact, EDC is able to couple carboxyl group with

primary amines, and its water solubility and the possibility to remove the excess by dialysis made this chemical way very attractive for such purposes.

After 20 min from the preparation of HA90/CTL47 coacervates, 50 µL of a 120 µg/mL solution of EDC were added drop-wise, followed by 50 µL of a 30 µg/mL solution of NHS (*N*-Hydroxysuccinimide). The latter reactant was used to increase the chemical stability of the reaction. Complex coacervates solution was let to proceed under gentle stirring for 3 h, allowing for the stabilization of the system. DLS analyses of the coacervates prepared with the cross-linking method were carried both at pH 4.5 and 7.4. In Figure 25 the size distributions of HA90/CTL47 coacervates in AcOH/AcNa buffer (pH 4.5) and in PBS (pH 7.4) are reported. Coacervates peaked at the same size (size at pH 4.5: 461 ± 67 nm; size at pH 7.4: 463 ± 3 nm) and displayed comparable homogeneity. The result clearly demonstrated that the use of EDC-NHS coupling fostered the stability of coacervates at physiological pH without altering their structure.

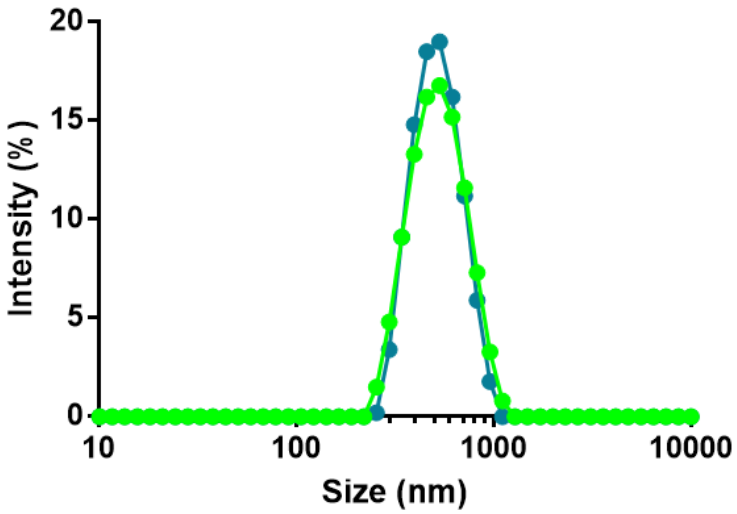

Figure 25: DLS investigation on the stability of HA90/CTL47 coacervates prepared with EDC/NHS coupling chemistry at pH 4.5 (green) and 7.4 (blue).

A preliminary evaluation of the biocompatibility of EDC-NHS coupled-coacervates was performed. Three different concentrations of coacervates were tested (Figure 26). MG-63 cells were seeded at day 0 and the proliferation was followed for three days. Figure 26 summarized the results: the cells seeded at pH 7.4 with the three different concentrations of coacervates displayed similar proliferation rate and no significant difference with respect to the control (cells seeded in plain medium). These results proved that HA/CTL coacervates did not affect cell proliferation *in vitro* and the concentration of EDC used for coacervates stabilization had no influence on cell viability.

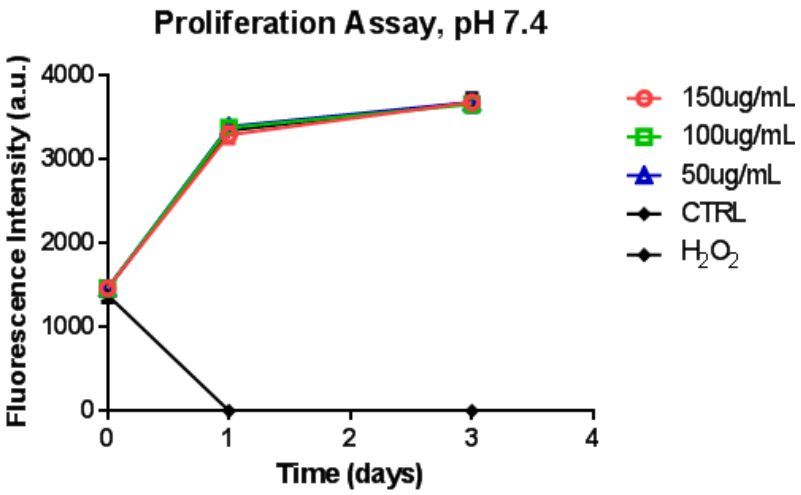

Figure 26: Cell proliferation of MG-63 cell line as a function of time. The cells were treated with three different amounts of coacervtes. Alamar Blue assay was performed after 4 hours, 1 and 3 days after the seeding. Results are reported as means (±SD, *n* =4).

CHAPTER 3: Preparation and characterization of Alginate/CTL/Chondroitin sulfate hydrogels

3.3.1 Aim of the work

This third chapter conclude the development of the biomaterial. Alginate, chondroitin sulfate and CTL were chosen for the preparation of a bioactive hydrogel. Rheological measurements were carried on to investigate the mechanical properties of this 3D structure. Subsequently, the possibility to successfully embed the coacervates into the hydrogel was evaluated by means of a confocal laser scanning microscope. The release of Dexamethasone from the coacervates embedded into the hydrogel was followed for 7 days, demonstrating the possibility to vehicle a therapeutic molecule with this system.

3.3.2. Materials and Methods

3.3.2.1. Materials

Alginate (F_G = 0.69; F_{GG} = 0.56; molecular weight (MW) = 130 000) was kindly provided by FMC biopolymers (Drammen, Norway). CTL (F_A= 0.16; F_D= 0.22, F_L= 0.62; η= 45.9 mPa) was kindly provided by BiopoLife s.r.l. Chondroitin sulfate (molecular weight = 463.363 g/mol), NaCl, $CaCl_2$, $MgCl_2$, $NaHCO_3$, K_2HPO_4 were purchased by Sigma Aldrich Chemical Co. (Milwaukee, WI). Deionized filtered water was used for the preparation of hydrogels.

3.3.2.3. Hydrogel preparation

Alg/CTL/CS hydrogels were prepared by exploiting an external gelation already reported for alginate and chitosan gels. [104] Alginate, CTL and chondroitin sulfate were dissolved separately in deionized filtered water at a final concentration of 1% (w/v), 0.5% (w/v) and 0.3% (w/v), respectively. The pH of the three solutions was adjusted to 7.4 using NaOH 1M. A constant ratio of 1:15 between

Hepes and NaCl was kept for all the solutions. CS and CTL were next added drop-wise to the Alg solution and allowed to mix homogenously. NaCl was used as supporting salt to provide a final ionic strength, *I*, of 0.15 M. The solution was casted into a mold (diameter = 22 mm, height = 2.5 mm) closed by two dialysis membranes (Molecular weight cut off ~ 12 000, average flat width 25 mm, Sigma Aldrich, Chemical Co.) and fixed by double circular stainless iron rings. The system was hermetically sealed and immersed into a 50 mM $CaCl_2$ solution (gelling bath, pH 7.4, NaCl 0.15 M). Ion diffusion proceed for 30 min under moderate stirring at room temperature.

3.3.2.4. Rheological measurements

Rheological characterization of cylindrical Alg/CTL/CS hydrogels was performed by means of controlled stress HAAKE MARS III rheometer (Thermo Scientific) operating at T = 25 °C using, as measuring device, a shagreened plate apparatus (HPP20 profiliert: diameter = 20 mm). To avoid water evaporation from the hydrogel, the measurements were performed in a water-saturated environment using a glass bell (solvent trap) containing a wet cloth. First, the gap between plates was adjusted by performing a series of short stress sweep tests (ν = 1 Hz; stress range 1 - 5 Pa; maximum deformation < 0.1%) in order to detect the optimum distance that allowed to maximize the elastic modulus, G', without causing excessive gel squeezing (which could reflect in the alteration of polymeric network properties). For each hydrogel, the linear viscoelastic range was determined by means of a stress sweep test consisting in measuring the elastic, G', and viscous, G'', moduli variation with increasing shear stress at a frequency, ν, of 1 Hz. On the same samples, stress relaxation (SR), creep recovery (CR) and long stress sweep (LSSW) tests were performed. In particular, during the stress relaxation test an instantaneous strain of 1% was applied and the stress decay was followed for 10 min; conversely, in the CR test, the hydrogel was allowed to creep during the imposition of a continuous stress for 15 min, after that the recovery of the hydrogel was fallowed for other 15 min.

3.3.2.5. Preparation of coacervates/hydrogel systems

HA/CTL47-FITC coacervates were prepared as described in section 3.1.2.3. HA/CTL47-FITC coacervates were dispersed in 2 mL of Alg/CTL/CS solutions and subsequently cast into a mold for gelation as described elsewhere. After 30 min, the hydrogel was retrieved from the gelling bath. A cross-section from the central part of the cylindrical hydrogel was obtained with a surgical scalpel and placed on a glass slide. The sample was mounted on the stage of an inverted microscope (Nikon C1 Standard Detector) associated with a confocal argon-ion laser scanning microscope. Laser excitation light was provided at a wavelength of 488 nm, and fluorescent emissions were collected at wavelengths between 510 nm and 580 nm. For the image acquisition, a Nikon Plan Fluor20X was used as objective. Confocal Laser Scanning Microscopy (CLSM) images were processed using ImageJ software.

3.3.2.6. Preparation of a Simulated Body Fluid (SBF)

The solution in which the hydrogel were placed for *in vitro* tests was SBF [105] with a pH of 7.4 and ion concentrations nearly equal to those of human blood plasma (Na^+ 142 mM , K^+ 5 mM, Mg^{2+} 1.5 mM, Ca^{2+} 2.5 mM , Cl^- 147.8 mM, HCO_3^- 4.2 mM, $HPO4^{2-}$ 1 mM, SO_4^{2-} 0.5 mM). The SBF was prepared by dissolving reagent-grade chemicals (NaCl, $NaHCO_3$, KCl, $K_2HPO_4 \cdot 3H_2O$, $MgCl_2 \cdot 6H_2O$, $CaCl_2$) in distilled water and buffering at pH 7.4 with tris(hydroxymethyl)aminomethane ($(CH_2OH)_3CNH_2$) and 1.0 M hydrochloric acid at 36.5 °C. SBF was sterilized with a 0.2 μm filter and stored between 2° and 8 °C for further use.

3.3.2.7. Swelling behavior of Alg/CTL/CS hydrogels

Swelling and dissolution behavior were investigated upon immersion of the hydrogels into SBF. Briefly, the specimens were cylindrical in shape with an average thickness of 2 mm and diameter of 23 mm. The swelling behavior was quantified by measuring the changes in sample weight as a function of soaking time in SBF. No erosion of hydrogels was observed throughout measurements. Wet weights

were determined after blotting with a filter paper to remove the surface liquid and the swelling ratio was calculated using the Equation (6):

$$E_{sr}(\%) = \left(\frac{w_s - w_d}{w_d}\right) * 100 \qquad (6)$$

where E_{sr} is the amount of absorbed water (weight percent) by the polymer matrix and W_d and W_s are the weights of the samples at time 0 and at the time of the measurements after soaking in SBF, respectively. The results were taken as the mean values of three measurements. The dimensions of the hydrogel prior and before the immersion were measured with a caliper. Soaking SBF was changed after each measurement.

3.3.2.8. Release of Dexamethasone

The release of dexamethasone from the hydrogel and from the coacervates/hydrogel system was measured in SBF. Dexamethasone was encapsulated at a final concentration of 20 μg/mL, and resulting coacervate dispersions was lyophilized as described before. The formation of coacervates/hydrogel system occurred as reported in section 3.3.2.3. Coacervate/hydrogel system was placed in 2 mL of SBF under shaking and the amount of released dexamethasone was quantified as indicated previously. The SBF was collected and replaced with fresh buffer after each investigated time. The coacervates/hydrogel system without dexamethasone were used as blank.

3.3.3 Results and discussion

Aiming at the preparation of a long lasting drug release-biomaterial, the loading of complex coacervates into a polymeric hydrogel was considered. Moreover, in order to fulfill the cartilage defect, the preparation of hydrogels with appropriate mechanics was explored.

Alginate (Alg), CTL and chondroitin sulfate (CS) were dissolved separately in deionized filtered water at a final concentration of 1%, 0.5% and 0.3% w/v respectively. The pH of the three polymers was adjusted to 7.4 using Hepes buffer (final concentration 10 mM) and NaOH 1 M, and NaCl (150 mM final concentration) was added for all the polymer solutions. Both the neutral pH and the presence of NaCl help to shield electrostatic interactions between CTL and Alginate in order to obtain a homogenous mixture rather than a phase separation.

The use of these three polymers has been already investigated for tissue engineering purposes. [106] [74] [107] [108] CTL and chondroition sulfate are both chosen for their bioactivity towards chondrocytes. On the other hand, alginate does not elicit any cellular response due to its lack of bioactivity, and does not provide any anchoring point for cellular adhesion; however, it is widely used for the preparation of 3D matrices when treated with gelling cations such as calcium or barium. In the present case, the formation of such matrices is achieved by means of an external gelation, simply termed “ion diffusion technique”, wherein polymers are initially separate from $CaCl_2$ bath. A schematic representation of the technique is reported in Figure 27.

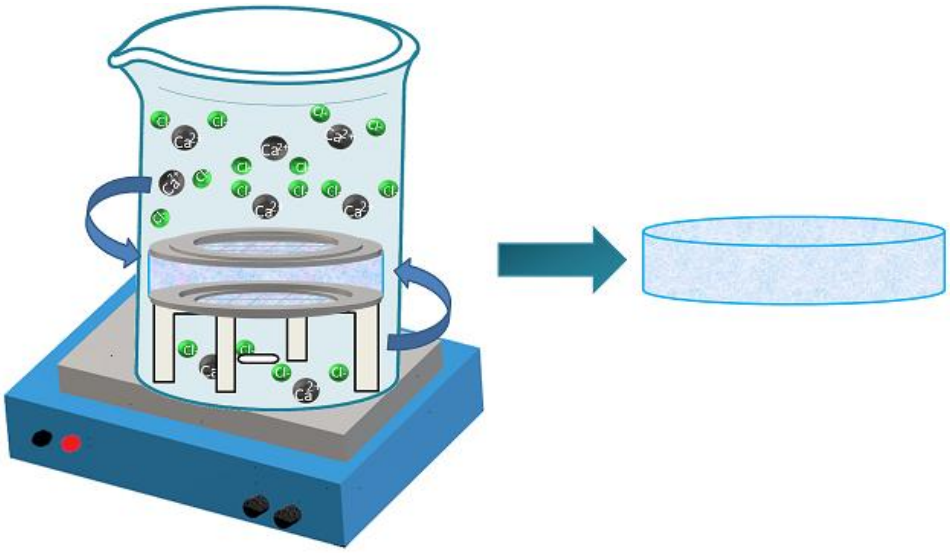

Figure 27: Schematic representation of the preparation of Alg/CTL/CS hydrogel exploiting the ion diffusion technique. A 50 mM $CaCl_2$ bath was used as gelling solution. Ca^{2+} ions diffused freely in and out the mold in which the Alg/CTL/CS solution is casted.

The Ca^{2+} ions are able to diffuse freely within polymer mixture upon external gelation starts. The presence of calcium interacting with alginate causes the almost immediate sol-gel transition of the polymer mixture. The (overall) effect is the formation of an ordered network. This property is at the root of both biological and industrial applications of alginates[109] [110]. In particular, the G-rich chains display high affinity for the divalent cations at very low concentration with respect to the M-rich chains. The explanation for such phenomenon lies in the secondary structure of alginates. The diaxial bond in homopolymeric chain of guluronates determines a curved fiber structure forming cavities, which facilitates the metal cation accommodation inside these negative cavities. The structure formed is reported in Figure 28, and it is commonly known as “egg-box”, in which one Ca^{2+} ion interacts with the G-blocks of two facing alginate chains.[111]

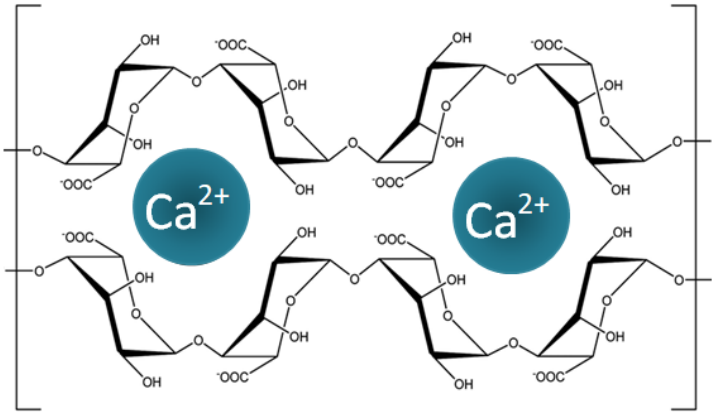

Figure 28: Schematic interaction of Ca^{2+} ions with the G-block of Alginate to form the so-called "egg box" structure.

The formation of hydrogels occurred within 30 min (Figure 29). Resulting systems appeared almost transparent, easy to handle and bend without breakage.

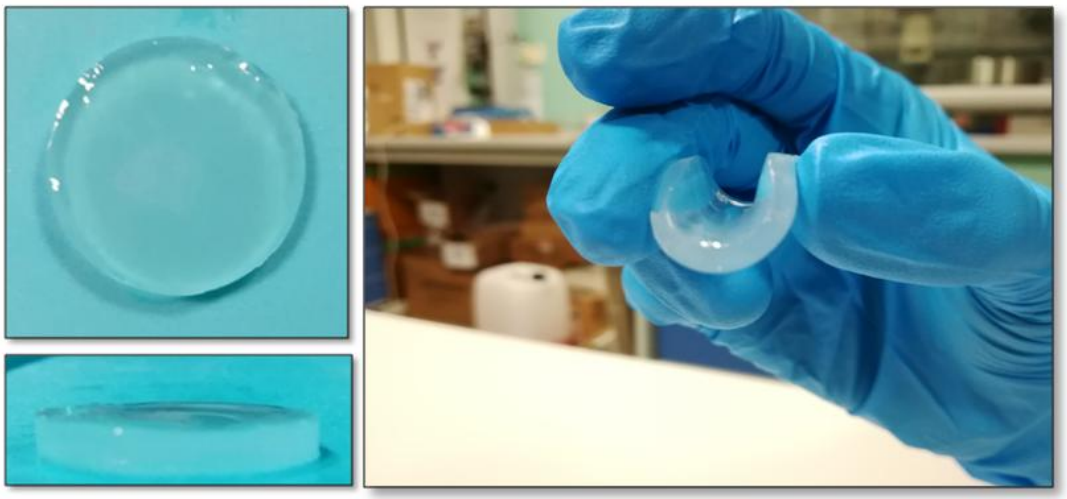

Figure 29: Alginate/CTL/chondroitin sulfate hydrogel

Hydrogels displayed a viscoelastic behavior if strained at small deformations. It is well known that articular cartilage withstands continuous shear and compressive stresses, and the distribution of load through the whole joint causes the deformation of the tissue. The particular composition of the ECM based on collagen and proteoglycans entraps water molecules and, at the

same time, allows polymer reptation to better distribute the load. An appropriate biomaterial for cartilage repair purposes should be able to mimic such mechanical characteristics.

Given these premises, different rheological measurements were performed to better understand the behavior of the biomaterial. First the mechanical spectrum of the hydrogel in oscillatory shear conditions was measured. Measurements were performed over a range of frequencies spanning from 0.01 to 100 Hz, T = 25 °C. For all the replicates measured, the storage modulus, G', was about tenfold the loss modulus, G'', and almost independent on the angular frequency for at least three decades, thus suggesting that the present system can be safely categorized as a strong hydrogel. The mechanical spectrum of one-case sample hydrogel is reported in Figure 30A The storage and loss moduli can be modeled in terms of the generalized Maxwell model - *i.e.* a combination of in parallel spring/dashpot elements - according to the following equations:

$$G' = G_e + \sum_{i=1}^{n} G_i \frac{(\lambda_i \omega)^2}{1+ (\lambda_i \omega)^2};\ G_i = \frac{\eta_i}{\lambda_i} \qquad (7)$$

$$G'' = \sum_{i=1}^{n} G_i \frac{\lambda_i \omega}{1+ (\lambda_i \omega)^2};\ G_i = \frac{\eta_i}{\lambda_i} \qquad (8)$$

where n is the number of Maxwell elements considered, G_i, η_i, and λ_i represent the spring constant, the dashpot viscosity, and the relaxation time of the ith Maxwell element, respectively. G_e is the spring constant supposed to be purely elastic. The fitting of the experimental data was performed assuming that relaxation times are not independent each other but they are scaled by a factor 10. Hence, the parameters of the model are G_e, η_i, and λ_1. The number of the Maxwell elements was selected, based on a statistical procedure, to minimize the product $\chi^2 * N_p$, where χ^2 is the sum of the squared errors, while N_p (= 2 + n) indicates the number of fitting parameters.

The use of Maxwell model enabled to calculate the shear modulus, G, which reflects the

stiffness of hydrogels under a constant stress at small deformations as

$$G = G_e + \sum_{i=1}^{n} G_i \ldots\ldots\ldots\ldots\ldots\ldots (9)$$

Resulting shear modulus, *G*, of the hydrogels was calculated to be approximately 20 kPa. This result is in line with other biomaterials proposed for cartilage tissue engineering [112], even if still lower mechanically compared to the native tissue.

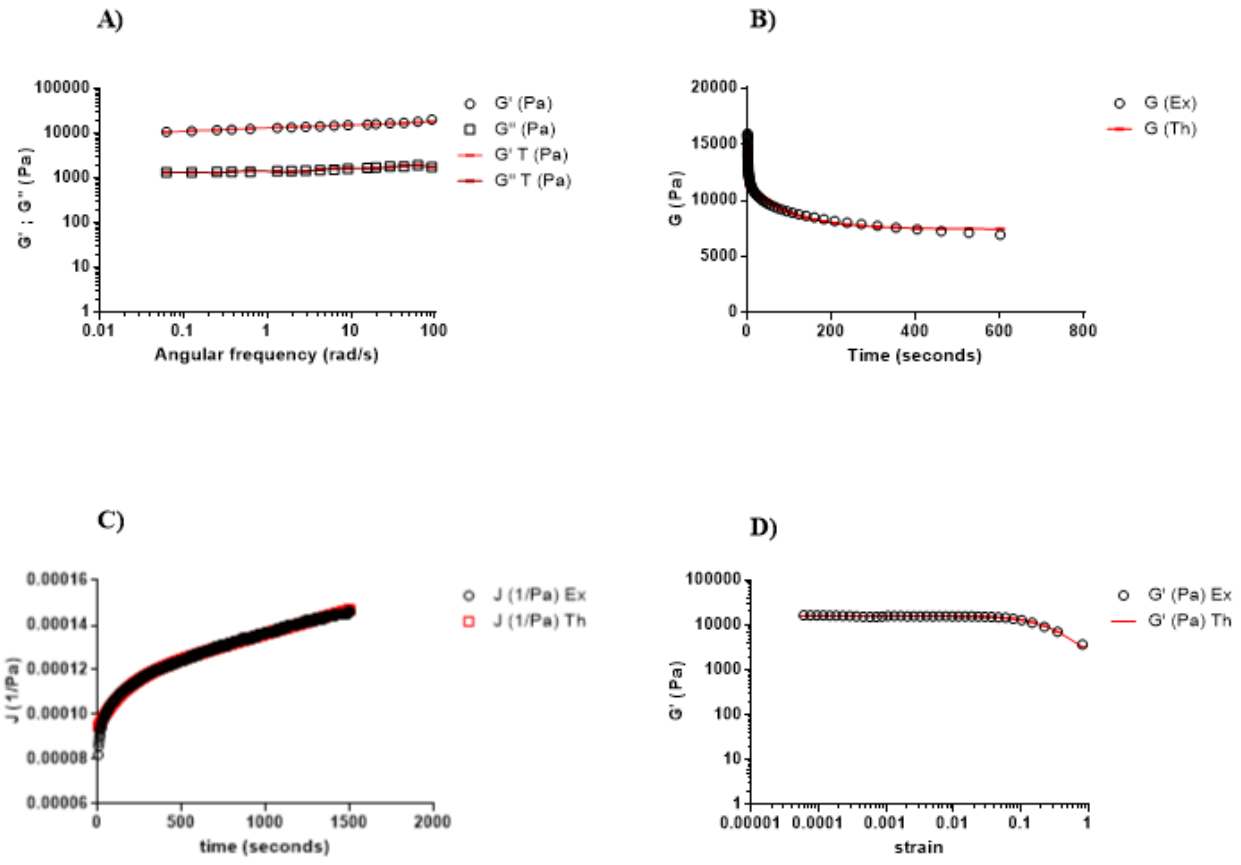

Figure 30: Panel reporting the rheological measurements on the hydrogel. A) Frequency sweep test, B) Stress relaxation test, C) Creep recovery test and D) Long stress sweep test.

To deeply investigate the mechanical behavior of hydrogels as a function of time, stress relaxation tests (SR) were performed The samples were undergone to an instantaneous strain, and

the stress decay was monitored over time (Figure 30B). This kind of test is very important also when considering materials that will be subjected to repetitive strain cycles, to determine if the stress can be dissipated over the time scale of tissue considered. As a matter of fact, the overloading in a material can cause damage and, therefore, negative clinical outcomes. [113] In particular, it was observed that the time needed to the material for relaxing the applied stress to half its value during the SR test (t_2) was about 1 s, whereas the t_1 was around 100 s. The former relaxation time refers to the initial fast decay whereas the latter one takes into account the slow (and modest) stress relaxation regime. The calculated values nicely fall into the relevant timescale at which cells respond to force oscillations, *i.e.* at which exert traction forces with ensuing spreading [114].

Hookean and Newtonian materials respond immediately after an applied stress, but when a viscoelastic material undergoes the same type of stress, it does not immediately respond with a constant flow, even though the stress may be sufficiently above the critical stress or yield point. When the stress is removed, this set of materials slowly recovers to almost their original state. This behavior is referred to as a creep. Figure 30C display the time dependency of the compliance *J*. After the sample was allowed to creep under load for about 30 min without squeezing,, the imposed stress was relieved, measuring the sample recover. The creep compliance was analyzed by means of a model composed of a Maxwell element in series with one Voigt element (eq 10), which accurately fitted all experimental data points

$$J(t) = J_0 + J_1\left(1 - e^{-t/\tau}\right) + \frac{t}{\eta_N} \quad \text{.....(10)}$$

where *J*(t) is the measured compliance, J_0 and J_1 are the compliances of the Maxwell and Voigt springs respectively, η_N is the so-called Newtonian viscosity of the Maxwell dashpot, and τ is the retardation time associated with the Voigt element. The resulted η_N was of about $5*10^7$ Pa*s. Such viscosity is related to the concentration of the polymer in the hydrogel and to the cross-linking density, so that the frictional forces between the chains connecting the junctions in the hydrogel can

explain the resistance of the network toward slipping. [115] It follows that the Newtonian viscosity of the hydrogel is directly proportional to the cross-linking density.

Long stress sweep tests were performed to verify the viscoelastic behavior of hydrogels at large deformation regime. This type of tests allows to detect the onset of non-linear regime at which the materials starts to soften. In Figure 30D it is reported the elastic modulus as a function of the strain. In the first region, it was observed an almost independency of G' on applied deformation, meaning that the stress scales linearly with the deformation. Above a critical strain value, a strain-softening profile was identified marking the onset of non-linear region. The critical strain at which the network started to weaken was approximately 3.5%.

The swelling capacity of the Alg/CTL/CS hydrogel was subsequently investigated. If an ionically cross-linked hydrogel is considered, we should recall that the present network typically rearrange its structure by absorbing the surrounding solvent (swelling behavior) or by expelling it (shrinking or deswelling behavior). The swelling - or conversely shrinking - properties depend on many factors such as network cross-linking density, solvent nature, polymer/solvent interactions. [116] The swelling capacity of the hydrogel was studied in physiological pH conditions using a Simulated Body Fluid (SBF) as medium for 7 days. The hydrogels were characterized by an initial swelling phase during the first 3 days, after that, a decrement of swelling ratio (%) was noticed. As a general consideration, the hydrogels seem to not degrade, however further investigations are required to exclude the potential release of singular polymer components, which might determine such a behavior.

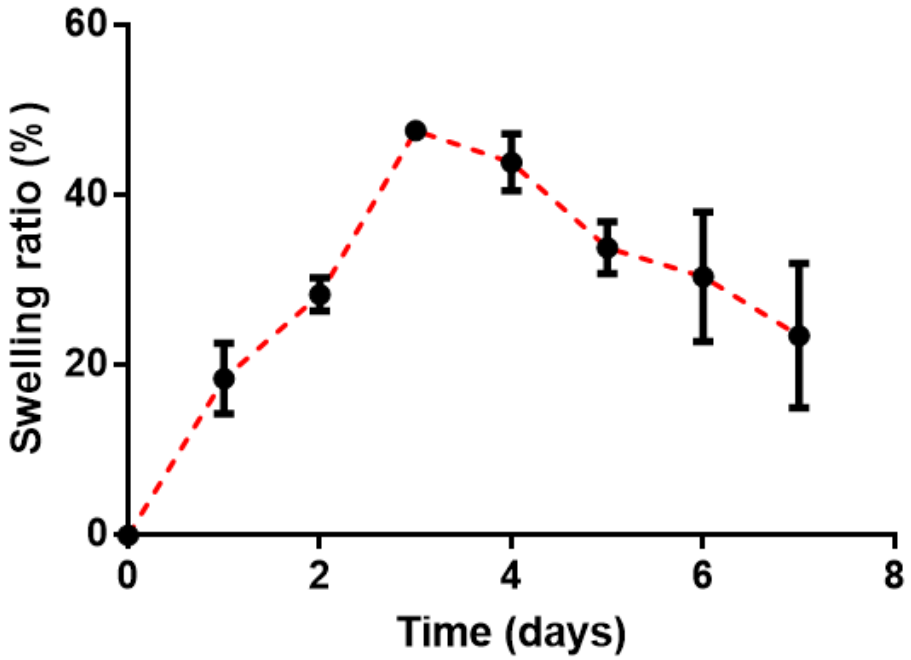

Figure 31: swelling ratio of Alg/CTL/CS hydrogel based on weight variation. Measurements were recorded from day 0 to day 7. For each sample the diameter, height and weight were measured. Data are reported as means (±SD, *n* = 3).

Scaffolds suitable for the controlled release of drug therapeutics have been studied, trying to solve the structural problems affecting articular cartilage. The combination of hydrogels with coacervates could favor a sustained and controlled release of one or more therapeutics or bioactive molecules. [117]

After the mechanical characterization of the hydrogel, it was hypothesized to combine the system with coacervates. HA90/CTL47-FITC coacervates were prepared using the EDC/NHS coupling chemistry. Coacervates were subsequently lyophilized as described previously, and then resuspended in 2 mL of Alg/CTL/CS solution and left under gentle stirring for about 10 min. Then, the whole mixture was gelled as described before.

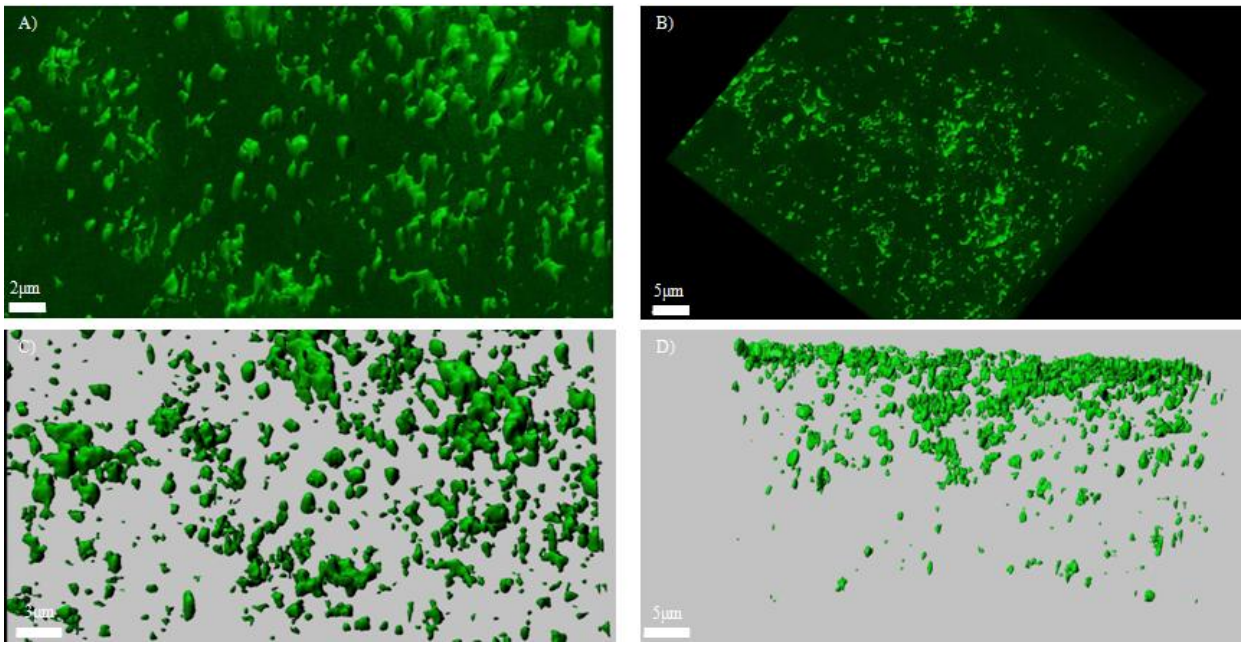

Figure 32: 3D rendering of complex coacervates embedded into an Alg/CTL/CS hydrogel. A) and C) top view of hydrogel section, B) and D) hydrogel cross section.

The hydrogel was recovered and cut along its cross-section; finally, it was placed on a microscope slide to observe the distribution of the coacervates within the hydrogel. The 3D rendering of the hydrogel was obtained by analyzing each Z-stack recorded by confocal laser scanning microscope analysis and reported in Figure 32. A slight auto-fluorescence of the hydrogel can be observed, likely due to CTL;. The coacervates, represented by green spots embedded in the hydrogel, can be clearly detected. This finding would suggest the possibility to successfully integrate coacervates within hydrogels. The distribution of the coacervates is not homogeneous, but they are mainly present at one side of the network. Such distribution could be attribute to an insufficient blending when the lyophilized coacervates were resuspended in the Alg/CTL/CS mixture. However, some important considerations can be drawn. The coacervates can be perfectly detected, retaining a sphere-like shape and a diameter comparable to not-embedded ones. Some aggregates are present, maybe ascribed to an insufficient blending, as previously discussed. The loading approach must be fine tuned in order to guarantee a better distribution of the coacervates and therefore an improvement of the whole system.

The successful loading of coacervates into the hydrogel matrix opened the way to the investigation of the whole system performance. In particular, given the final aim of this work to promote the release of therapeutics, the leakage of Dexamethasone from the coacervates embedded into the hydrogel was studied.

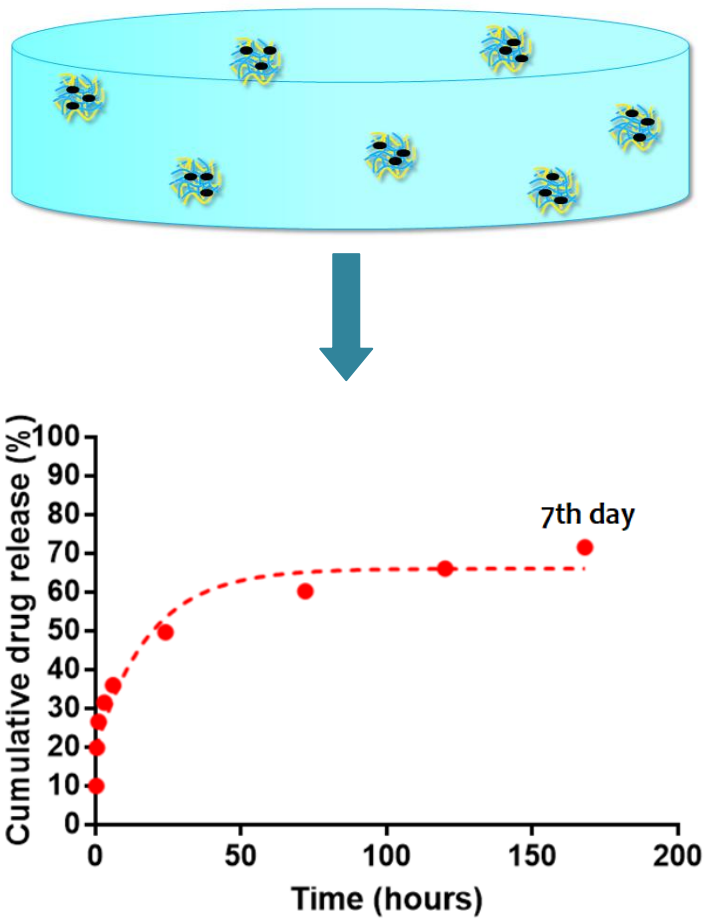

Figure 33: Cumulative drug release of Dexamethasone from coacervetas embedded into Alg/CTL/CS hydrogel. The release was followed up to 7 days.

HA90/CTL47/DEXA coacervates were prepared as described in paragraph 3.2.2.5 and subsequently embedded into the Alg/CTL/CS hydrogel. The system was placed in SBF and the release of Dexamethasone was followed at selected time points for one week. The cumulative drug release expressed as percentage is reported in Figure 33. An initial burst release was detected in the first hour, probably due to the leakage of free payload not encapsulated within coacervates, with the

50% of the drug released in 24 h. After 7 days, the release of dexamethasone was about 76%. Giving the integrity of the hydrogel after this period of time, it is hypothesized that the dexamethasone was not completely released. Such result supports the possibility to efficiently encapsulate molecule therapeutics in order to favor the controlled release over a prolonged period of time. In fact, if we compared the release from the single coacervate system (4 h) with that of the complete system (7 days), a prolonged release is clearly evident.

4. CONCLUSIONS

Nowadays, the regeneration of articular cartilage defect is still a great challenge. The lack of innervations, lymphatic and blood stream and the poor proliferation ability of chondrocytes prevent an appropriate regeneration of the tissue. Sports trauma, long term wear, ageing, obesity and genetic diseases can lead to cartilage and bone lesions that refer to arthritic diseases. Numerous approaches are employed to treat such diseases, based on the severity of the lesions (from the weight control, to visco-supplementation and surgical procedures). Unfortunately, none of them are able to restore the native tissue. For these reasons, researchers are exploring the tissue engineering approach which combines the use of biomaterials (3D structures), cells and bioactive molecules in order to regenerate damage tissues.

The goal of this project fall in this scenario, aiming at the development of a bioactive biomaterial that could fulfill the cartilage defect and promote the repair of the tissue. The structure of such biomaterial is designed like a polymeric hydrogel embedding drug-loaded complex coacervates in for a long term drug release.

It was first investigated the possibility to form complex coacervates by exploiting the electrostatic interaction between two oppositely charged polysaccharides, namely CTL and Hyaluronan. The behavior of such polymers when mixed together was studied, analyzing the influence of pH, ionic strength, polymer mixing, molecular weight and charge density. A complete miscibility of the two mentioned polymers was achieved at pH 7.4 for all the ionic strengths analyzed. As a matter of fact, CTL is almost uncharged in this pH condition, preventing the formation of complex coacervates. By decreasing the pH to 4.5, an increased turbidity of the system marked the formation of coacervates. By theoretical calculation and ζ-potential analyses it was observed that when the ratio of the two polymer is equal to one, the formation of precipitates without coacervates in solution occurs. Moreover, preliminary DLS analyses displayed the

formation of spherical particles for solution prepared with negligible ionic strength, underlined the influence of the molecular weight and the weight fraction of the polymers for coacervates preparation.

The possibility to obtain spheroidal nano-/microparticles when HA was added to CTL in the presence of a physiological concentration (*i.e.*, 150 mM) of NaCl was demonstrated, thereby overcoming screening phenomena. Interestingly, it was not only found that the supporting salt was unable to completely screen electrostatic attractive interactions, but it was even showed that it helped the reduction of the size distribution of coacervates. Time dissolution stability studies proved that coacervates did not dissolve at 37 °C up to 3 weeks; conversely, they disentangled upon increasing pH toward neutrality. Interestingly, the rate of dissolution could be tuned, to some extent, by varying CTL chemical composition, thus proving the usefulness of exploiting HA for stabilizing CTL- based colloids, with respect to and at variance with tripolyphosphate (TPP). The selected systems displayed suitable encapsulation efficiency, exhibited optimal drug loading, and preserved physical properties after freeze-drying in the presence of trehalose as cryoprotectant. Biological experiments using human neutrophils as cellular model pointed out the ability of HA/CTL coacervates to exert a significant ROS scavenging activity. Overall, the present findings - together with the documented bioactivity of CTL - suggest that the complex coacervation between CTL and low molecular weight hyaluronan can be considered as an effective strategy to form bioactive carriers to be used for the delivery of drugs toward confined inflamed sites known to be commonly associated with extracellular acidosis.

The stability of HA/CTL coacervates in physiological pH was achieved by taking advantage of the amino coupling. Biological evaluation demonstrate the compatibility of the coacervates, allowing their used for further studies. We prepared bioactive hydrogels based on alginate, CTL and chodroitin sulfate. The last two polymers had already demonstrate their influence on chondrocytes proliferation and matrix deposition, whereas alginate is currently used in many biological and

industrial application for its gel forming ability. Alginate/CTL/chondroitin sulfate hydrogel was formed by casting the polymers solution in a mold and diving in a $CaCl_2$ bath, exploiting the ion diffusion technique. Rheological characterizations of the hydrogel shown a behavior similar to other biomaterials proposed for similar applications. Although the distribution of coacervates within the hydrogel was not homogeneous, the possibility to successfully embed the coacervate into the hydrogel was stated using confocal laser scanning microscopy. Such achievement had opened the way to the investigation of the release of Dexamethasone from the complex system (dexamethasone-loaded coacervates embedded in the hydrogel). The release was followed for 7days. After an initial burst release, almost the 80% of dexamethasone was release within the time of observation. By comparing the release from the coacervates s with the complex system, an extension of the releasing time can be observed.

As future activities, a biological characterization, *in vitro* and *in vivo*, of the complex system will be considered, but the data collected in this three year work presents a valuable biomaterial for drug delivery, but also as vehicle of growth factors or other biologically active molecules.

BIBLIOGRAPHY

[1] D. Correa, S.A. Lietman, Articular cartilage repair: Current needs, methods and research directions, Semin. Cell Dev. Biol. 62 (2017) 67–77. doi:10.1016/j.semcdb.2016.07.013.

[2] A.J. Sophia Fox, A. Bedi, S.A. Rodeo, The Basic Science of Articular Cartilage: Structure, Composition, and Function, Sport. Heal. A Multidiscip. Approach. 1 (2009) 461–468. doi:10.1177/1941738109350438.

[3] C. Vinatier, J. Guicheux, Cartilage tissue engineering: From biomaterials and stem cells to osteoarthritis treatments, Ann. Phys. Rehabil. Med. 59 (2016) 139–144. doi:10.1016/j.rehab.2016.03.002.

[4] J. Martel-Pelletier, A.J. Barr, F.M. Cicuttini, P.G. Conaghan, C. Cooper, M.B. Goldring, S.R. Goldring, G. Jones, A.J. Teichtahl, J.-P. Pelletier, Osteoarthritis, Nat. Rev. Dis. Prim. 2 (2016) 16072. doi:10.1038/nrdp.2016.72.

[5] G. Jones, C. Ding, M. Glisson, K. Hynes, D. Ma, F. Cicuttini, Knee articular cartilage development in children: A longitudinal study of the effect of sex, growth, body composition, and physical activity, Pediatr. Res. 54 (2003) 230–236. doi:10.1203/01.PDR.0000072781.93856.E6.

[6] C. Rodriguez-Fontenla, M. Calaza, E. Evangelou, A.M. Valdes, N. Arden, F.J. Blanco, A. Carr, K. Chapman, P. Deloukas, M. Doherty, T. Esko, C.M. Garcés Aletá, J.J. Gomez-Reino Carnota, H. Helgadottir, A. Hofman, I. Jonsdottir, H.J.M. Kerkhof, M. Kloppenburg, A. McCaskie, E.E. Ntzani, W.E.R. Ollier, N. Oreiro, K. Panoutsopoulou, S.H. Ralston, Y.F. Ramos, J.A. Riancho, F. Rivadeneira, P.E. Slagboom, U. Styrkarsdottir, U. Thorsteinsdottir, G. Thorleifsson, A. Tsezou, A.G. Uitterlinden, G.A. Wallis, J.M. Wilkinson, G. Zhai, Y. Zhu, D.T. Felson, J.P.A. Ioannidis, J. Loughlin, A. Metspalu, I. Meulenbelt, K. Stefansson,

J.B. Van Meurs, E. Zeggini, T.D. Spector, A. Gonzalez, Assessment of osteoarthritis candidate genes in a meta-analysis of nine genome-wide association studies, Arthritis Rheumatol. 66 (2014) 940–949. doi:10.1002/art.38300.

[7] T.D. Spector, F. Cicuttini, J. Baker, J. Loughlin, D. Hart, Genetic influences on osteoarthritis in women: a twin study, Bmj. 312 (1996) 940–943. doi:10.1136/bmj.312.7036.940.

[8] C. Maes, E. Araldi, K. Haigh, R. Khatri, R. Van Looveren, A.J. Giaccia, J.J. Haigh, G. Carmeliet, E. Schipani, VEGF-independent cell-autonomous functions of HIF-1α regulating oxygen consumption in fetal cartilage are critical for chondrocyte survival, J. Bone Miner. Res. 27 (2012) 596–609. doi:10.1002/jbmr.1487.

[9] K. Mithoefer, R.J. Williams, R.F. Warren, H.G. Potter, C.R. Spock, E.C. Jones, T.L. Wickiewica, R.G. Marx, the Microfracture Technique for the Treatment of Articular Cartilage lesion in the knee, J. BONE Jt. Surg. 87–A (2005) 1911–1920.

[10] T.J. Gill, P.D. Asnis, E.M. Berkson, The Treatment of Articular Cartilage Defects Using the Microfracture Technique, J. Orthop. Sport. Phys. Ther. 36 (2006) 728–738. doi:10.1016/S1048-6666(01)80019-7.

[11] A. Carranza-Bencano, M. Perez-Tinao, P. Ballesteros-Vazquez, J.R. Armas-Padron, A. Hevia-Alonso, F. Martos Crespo, Comparative study of the reconstruction of articular cartilage defects with free costal perichondrial grafts and free tibial periosteal grafts: An experimental study on rabbits, Calcif. Tissue Int. 65 (1999) 402–407. doi:10.1007/s002239900721.

[12] M.F. Erol, O. Karakoyun, A new point of view for mosaicplasty in the treatment of focal cartilage defects of knee joint: honeycomb pattern, Springerplus. 5 (2016). doi:10.1186/s40064-016-2796-y.

[13] M. Marcacci, E. Kon, S. Zaffagnini, F. Iacono, M.P. Neri, A. Vascellari, A. Visani, A. Russo, Multiple osteochondral arthroscopic grafting (mosaicplasty) for cartilage defects of the knee: prospective study results at 2-year follow-up., Arthroscopy. 21 (2005) 462–470. doi:10.1016/j.arthro.2004.12.003.

[14] L. Hangody, G. Kish, Z. Kárpáti, I. Szerb, I. Udvarhelyi, Arthroscopic autogenous osteochondral mosaicplasty for the treatment of femoral condylar articular defects: A preliminary report, Knee Surgery, Sport. Traumatol. Arthrosc. 5 (1997) 262–267. doi:10.1007/s001670050061.

[15] L. Hangody, P. Füles, Autologous osteochondral mosaicplasty for the treatment of full-thickness defects of weight-bearing joints: Ten years of experimental and clinical experience, J. Bone Jt. Surg. - Ser. A. 85 (2003) 25–32. doi:10.2106/00004623-200300002-00004.

[16] D. a Grande, M.I. Pitman, L. Peterson, D. Menche, M. Klein, The repair of experimentally produced defects in rabbit articular cartilage by autologous chondrocyte transplantation, J. Orthop. Res. 7 (1989) 208–218. doi:10.1002/jor.1100070208.

[17] J.P. G. Bentley, L. C. Biant, R. W. J. Carrington, M. Akmal, A. Goldberg, A. M. Williams, J. A. Skinner, A prospective, randomised comparison of autologous chondrocyte implantation versus mosaicplasty for osteochondral defects in the knee, J. BONE Jt. Surg. 85 (2003) 1–6. doi:10.1302/0301-620X.85B2.13543.

[18] O.I. and L.P. M. Brittberg, A. Lindahl, A. Nilsson, C. Ohlsson, Treatment of deep cartilage defects in the knee with autologous chondrocyte transplantation, N. Engl. J. Med. 331 (1994) 889–895. doi:10.1007/s40262-012-0001-1.

[19] J. Martel-Pelletier, A.J. Barr, F.M. Cicuttini, P.G. Conaghan, C. Cooper, M.B. Goldring, S.R. Goldring, G. Jones, A.J. Teichtahl, J.P. Pelletier, Osteoarthritis, Nat. Rev. Dis. Prim. 2

(2016). doi:10.1038/nrdp.2016.72.

[20] R. Langer, J.P. Vacanti, Tissue Engineering, Science (80-.). 260 (1993) 920–926. doi:10.1126/science.8493529.

[21] Y. Liu, G. Zhou, Y. Cao, Recent Progress in Cartilage Tissue Engineering—Our Experience and Future Directions, Engineering. 3 (2017) 28–35. doi:10.1016/J.ENG.2017.01.010.

[22] N.O.S.C. Bassi, Ênio José Carlos Alberto Mayora Aita, Ênio, Immune regulatory properties of multipotent mesenchymal stromal cells: Where do we stand?, World J. Stem Cells. 3 (2011) 1–8. doi:10.4252/wjsc.v3.i1.1.

[23] T. Yuan, L. Zhang, K. Li, H. Fan, Y. Fan, J. Liang, X. Zhang, Collagen hydrogel as an immunomodulatory scaffold in cartilage tissue engineering, J. Biomed. Mater. Res. - Part B Appl. Biomater. 102 (2014) 337–344. doi:10.1002/jbm.b.33011.

[24] P.C. Kreuz, C. Gentili, B. Samans, D. Martinelli, J.P. Krüger, W. Mittelmeier, M. Endres, R. Cancedda, C. Kaps, Scaffold-assisted cartilage tissue engineering using infant chondrocytes from human hip cartilage, Osteoarthr. Cartil. 21 (2013) 1997–2005. doi:10.1016/j.joca.2013.09.007.

[25] N. Monteiro, A. Martins, R.L. Reis, N.M. Neves, Nanoparticle-based bioactive agent release systems for bone and cartilage tissue engineering, Regen. Ther. 1 (2015) 109–118. doi:10.1016/j.reth.2015.05.004.

[26] B.J. Huang, J.C. Hu, K.A. Athanasiou, Cell-based tissue engineering strategies used in the clinical repair of articular cartilage, Biomaterials. 98 (2016) 1–22. doi:10.1016/j.biomaterials.2016.04.018.Cell-based.

[27] J. Malmo, K.M. Vårum, S.P. Strand, Effect of Chitosan Chain Architecture on Gene Delivery: Comparison of Self-Branched and Linear Chitosans, Biomacromolecules. 12

(2011) 721–729. doi:10.1021/bm1013525.

[28] J. Malmo, H. Sørgård, K.M. Vårum, S.P. Strand, siRNA delivery with chitosan nanoparticles: Molecular properties favoring efficient gene silencing, J. Control. Release. 158 (2012) 261–268. doi:10.1016/j.jconrel.2011.11.012.

[29] Y. Li, B. Humphries, Z. Wang, S. Lang, X. Huang, H. Xiao, Y. Jiang, C. Yang, Complex Coacervation-Integrated Hybrid Nanoparticles Increasing Plasmid DNA Delivery Efficiency *in Vivo*, ACS Appl. Mater. Interfaces. 8 (2016) 30735–30746. doi:10.1021/acsami.6b10306.

[30] P. Sacco, E. Decleva, F. Tentor, R. Menegazzi, M. Borgogna, S. Paoletti, K.A. Kristiansen, K.M. Vårum, E. Marsich, Butyrate-Loaded Chitosan/Hyaluronan Nanoparticles: a Suitable Tool for Sustained Inhibition of ROS Release by Activated Neutrophils, Macromol. Biosci. 1700214 (2017). doi:10.1002/mabi.201700214.

[31] H.J. Li Hongshuai, Johnson Noah Ray, Usas Arvydas, Lu Aiping, Poddar Minakshi, Wang Yadong, Sustained Release of Bone Morphogenetic Protein 2 via Coacervate Improves the Osteogenic Potential of Muscle-Derived Stem Cells, Stem Cells Transl. Med. 2 (2013) 667–677.

[32] A.B. Kayitmazer, A.F. Koksal, E. Kilic Iyilik, Complex coacervation of hyaluronic acid and chitosan: effects of pH, ionic strength, charge density, chain length and the charge ratio, Soft Matter. 11 (2015) 8605–8612. doi:10.1039/C5SM01829C.

[33] E. Lallana, J.M. Rios De La Rosa, A. Tirella, M. Pelliccia, A. Gennari, I.J. Stratford, S. Puri, M. Ashford, N. Tirelli, Chitosan/Hyaluronic Acid Nanoparticles: Rational Design Revisited for RNA Delivery, Mol. Pharm. 14 (2017) 2422–2436. doi:10.1021/acs.molpharmaceut.7b00320.

[34] A.F. Martins, D.M. de Oliveira, A.G.B. Pereira, A.F. Rubira, E.C. Muniz, Chitosan/TPP

microparticles obtained by microemulsion method applied in controlled release of heparin, Int. J. Biol. Macromol. 51 (2012) 1127–1133. doi:10.1016/j.ijbiomac.2012.08.032.

[35] J.T. Oliveira, R.L. Reis, Hydrogels from polysaccharide-based materials: Fundamentals and applications in regenerative medicine, Woodhead Publ. Ser. Biomater. (2008) 485–514. doi:10.1533/9781845694814.4.485.

[36] S. Sugiura, T. Oda, Y. Izumida, Y. Aoyagi, M. Satake, A. Ochiai, N. Ohkohchi, M. Nakajima, Size control of calcium alginate beads containing living cells using micro-nozzle array, Biomaterials. 26 (2005) 3327–3331. doi:10.1016/j.biomaterials.2004.08.029.

[37] H.H. Tønnesen, J. Karlsen, Alginate in drug delivery systems, Drug Dev. Ind. Pharm. 28 (2002) 621–630. doi:10.1081/DDC-120003853.

[38] Y. Xu, C. Zhan, L. Fan, L. Wang, H. Zheng, Preparation of dual crosslinked alginate-chitosan blend gel beads and in vitro controlled release in oral site-specific drug delivery system, Int. J. Pharm. 336 (2007) 329–337. doi:10.1016/j.ijpharm.2006.12.019.

[39] A.A. Badwan, A. Abumalooh, E. Sallam, A. Abukalaf, O. Jawan, A sustained release drug delivery system using calcium alginate beads, Drug Dev. Ind. Pharm. 11 (1985) 239–256. doi:10.3109/03639048509056869.

[40] P. Sacco, F. Brun, I. Donati, D. Porrelli, S. Paoletti, G. Turco, On the Correlation between the Microscopic Structure and Properties of Phosphate-Cross-Linked Chitosan Gels, ACS Appl. Mater. Interfaces. 10 (2018) 10761–10770. doi:10.1021/acsami.8b01834.

[41] P. Sacco, M. Cok, F. Asaro, S. Paoletti, I. Donati, The role played by the molecular weight and acetylation degree in modulating the stiffness and elasticity of chitosan gels, Carbohydr. Polym. 196 (2018) 405–413. doi:10.1016/j.carbpol.2018.05.060.

[42] M. Cok, P. Sacco, D. Porrelli, A. Travan, M. Borgogna, E. Marsich, S. Paoletti, I. Donati,

Mimicking mechanical response of natural tissues. Strain hardening induced by transient reticulation in lactose-modified chitosan (chitlac), Int. J. Biol. Macromol. 106 (2018) 656–660. doi:10.1016/j.ijbiomac.2017.08.059.

[43] A. Deng, X. Kang, J. Zhang, Y. Yang, S. Yang, Enhanced gelation of chitosan/β-sodium glycerophosphate thermosensitive hydrogel with sodium bicarbonate and biocompatibility evaluated, Mater. Sci. Eng. C. 78 (2017) 1147–1154. doi:10.1016/j.msec.2017.04.109.

[44] C.L. Huang, Y. Bin Chen, Y.L. Lo, Y.H. Lin, Development of chitosan/β-glycerophosphate/glycerol hydrogel as a thermosensitive coupling agent, Carbohydr. Polym. 147 (2016) 409–414. doi:10.1016/j.carbpol.2016.04.028.

[45] T.M. Tamer, Hyaluronan and synovial joint: Function, distribution and healing, Interdiscip. Toxicol. 6 (2013) 111–125. doi:10.2478/intox-2013-0019.

[46] G. Kogan, L. Soltes, R. Stern, P. Gemeiner, Hyaluronic acid : a natural biopolymer with a broad range of biomedical and industrial applications, Biotechnol Lett. 29 (2007) 17–25. doi:10.1007/s10529-006-9219-z.

[47] M. Viola, D. Vigetti, E. Karousou, M.L. D'Angelo, I. Caon, P. Moretto, G. De Luca, A. Passi, Biology and biotechnology of hyaluronan, Glycoconj. J. 32 (2015) 93–103. doi:10.1007/s10719-015-9586-6.

[48] C. Longinotti, The use of hyaluronic acid based dressings to treat burns: A review, Burn. Trauma. 2 (2014) 162. doi:10.4103/2321-3868.142398.

[49] C. Cindy, B. Jason, Influence of 3D Hyaluronic Acid Microenvironments on Mesenchymal Stem Cell Chondrogenesis, Tissue Eng Part A. 15 (2009) 243–254. doi:10.1089/ten.tea.2008.0067.Influence.

[50] J.Y. Chung, M. Song, C.W. Ha, J.A. Kim, C.H. Lee, Y.B. Park, Comparison of articular

cartilage repair with different hydrogel-human umbilical cord blood-derived mesenchymal stem cell composites in a rat model, Stem Cell Res. Ther. 5 (2014) 1–13. doi:10.1186/scrt427.

[51] L. Calderon, E. Collin, D. Velasco-Bayon, M. Murphy, D. O'Halloran, A. Pandit, Type II Collagen-Hyaluronan Hydrogel - A Step Towards A Scaffold For Intervertebral Disc Tissue Engineering, Eur. Cells Mater. 20 (2010) 134–148. doi:10.22203/eCM.v020a12.

[52] M.R.L. Minwook Kim, Erickson Isaac E., Choudhury Marwa, Pleshko Nancy, Transient exposure to TGF-β3 improves the functional chondrogenesis of MSC-laden hyaluronic acid hydrogels, J Mech Behav Biomed Mater. 11 (2012) 92–101. doi:10.1038/jid.2014.371.

[53] M.N.V.R. Kumar, A review of chitin and chitosan applications, Eng. Sci. Fundam. 2015 - Core Program. Area 2015 AIChE Annu. Meet. 46 (2000) 1–27. doi:10.1016/S1381-5148(00)00038-9.

[54] V.K. Mourya, N.N. Inamdar, Chitosan-modifications and applications: Opportunities galore, React. Funct. Polym. 68 (2008) 1013–1051. doi:10.1016/j.reactfunctpolym.2008.03.002.

[55] M. Yalpani, L.D. Hall, Some Chemical and Analytical Aspects Of Polysaccharide Modifications. Formation of Branched-Chain, Soluble Chitosan Derivatives, Macromolecules. 17 (1984) 272–281. doi:10.1021/ma00133a003.

[56] N. D'Amelio, C. Esteban, A. Coslovi, L. Feruglio, F. Uggeri, M. Villegas, J. Benegas, S. Paoletti, I. Donati, Insight into the molecular properties of chitlac, a chitosan derivative for tissue engineering, J. Phys. Chem. B. 117 (2013) 13578–13587. doi:10.1021/jp4067263.

[57] I. Donati, I.J. Huag, T. Scarpa, M. Borgogna, K.I. Draget, G. Skjåk-Bræk, S. Paoletti, Synergistic effects in semidilute mixed solutions of alginate and lactose-modified chitosan (chitlac), Biomacromolecules. 8 (2007) 957–962. doi:10.1021/bm060856h.

[58] M. Di Giulio, S. Di Bartolomeo, E. Di Campli, S. Sancilio, E. Marsich, A. Travan, A. Cataldi, L. Cellini, The effect of a silver nanoparticle polysaccharide system on streptococcal and saliva-derived biofilms, Int. J. Mol. Sci. 14 (2013) 13615–13625. doi:10.3390/ijms140713615.

[59] A. Travan, I. Donati, E. Marsich, F. Bellomo, S. Achanta, M. Toppazzini, S. Semeraro, T. Scarpa, V. Spreafico, S. Paoletti, Surface modification and polysaccharide deposition on BisGMA/TEGDMA thermoset, Biomacromolecules. 11 (2010) 583–592. doi:10.1021/bm9011419.

[60] E. Marsich, M. Borgogna, I. Donati, P. Mozetic, B.L. Strand, S.G. Salvador, F. Vittur, S. Paoletti, Alginate/lactose-modified chitosan hydrogels: a bioactive biomaterial for chindrocyte encapsulation, Clin. Exp. Rheumatol. Biomed. Mater. Res. Part A. 84A (2007) 365–376. doi:10.1002/jbm.a.

[61] F. Furlani, P. Sacco, E. Marsich, I. Donati, S. Paoletti, Highly monodisperse colloidal coacervates based on a bioactive lactose-modified chitosan: From synthesis to characterization, Carbohydr. Polym. 174 (2017) 360–368. doi:10.1016/j.carbpol.2017.06.097.

[62] P. Marcon, E. Marsich, A. Vetere, P. Mozetic, C. Campa, I. Donati, F. Vittur, A. Gamini, S. Paoletti, The role of Galectin-1 in the interaction between chondrocytes and a lactose-modified chitosan, Biomaterials. 26 (2005) 4975–4984. doi:10.1016/j.biomaterials.2005.01.044.

[63] P. Sacco, F. Furlani, M. Cok, A. Travan, M. Borgogna, E. Marsich, S. Paoletti, I. Donati, Boric Acid Induced Transient Cross-Links in Lactose-Modified Chitosan (Chitlac), Biomacromolecules. 18 (2017) 4206–4213. doi:10.1021/acs.biomac.7b01237.

[64] E.C.C. Stanford, On Algin, a new substance obtained from some of the commoner species of marine algae, Chem. News. 2 (1883) 254–257.

[65] G.T. Grant, E.R. Morris, D.A. Rees, P.J.C. Smith, D. Thom, Biological interactions between polysaccharides and divalent cations: The egg-box model, FEBS Lett. 32 (1973) 195–198. doi:10.1016/0014-5793(73)80770-7.

[66] G. Turco, E. Marsich, F. Bellomo, S. Semeraro, I. Donati, F. Brun, M. Grandolfo, A. Accardo, S. Paoletti, Alginate/hydroxyapatite biocomposite for bone ingrowth: A trabecular structure with high and isotropic connectivity, Biomacromolecules. 10 (2009) 1575–1583. doi:10.1021/bm900154b.

[67] D. Porrelli, A. Travan, G. Turco, E. Marsich, M. Borgogna, S. Paoletti, I. Donati, Alginate-Hydroxyapatite Bone Scaffolds with Isotropic or Anisotropic Pore Structure: Material Properties and Biological Behavior, Macromol. Mater. Eng. 300 (2015) 989–1000. doi:10.1002/mame.201500055.

[68] H.-L. Ma, S.-C. Hung, S.-Y. Lin, Y.-L. Chen, W.-H. Lo, Chondrogenesis of human mesenchymal stem cells encapsulated in alginate beads, J. Biomed. Mater. Res. 64A (2003) 273–281. doi:10.1002/jbm.a.10370.

[69] L. Wang, E. Khor, A. Wee, L.Y. Lim, Chitosan-alginate PEC membrane as a wound dressing: Assessment of incisional wound healing, J. Biomed. Mater. Res. 63 (2002) 610–618. doi:10.1002/jbm.10382.

[70] P. Li, Y.-N. Dai, J.-P. Zhang, A.-Q. Wang, Q. Wei, Chitosan-alginate nanoparticles as a novel drug delivery system for nifedipine., Int. J. Biomed. Sci. 4 (2008) 221–8. http://www.pubmedcentral.nih.gov/articlerender.fcgi?artid=3614711&tool=pmcentrez&rendertype=abstract.

[71] T. Omata, Y. Itokazu, N. Inoue, Y. Segawa, Effects of Chondroitin Sulfate-C on Articular Cartilage Destruction in Murine Collagen-induced Arthritis, Arzneimittelforschung. 50 (2000) 148–153. doi:10.1055/s-0031-1300180.

[72] Y. Henrotin, M. Mathy, C. Sanchez, C. Lambert, Chondroitin sulfate in the treatment of osteoarthritis: From in vitro studies to clinical recommendations, Ther. Adv. Musculoskelet. Dis. 2 (2010) 335–348. doi:10.1177/1759720X10383076.

[73] D. Uebelhart, Clinical review of chondroitin sulfate in osteoarthritis, Osteoarthr. Cartil. 16 (2008) 19–21. doi:10.1016/j.joca.2008.06.006.

[74] R.A.A. Muzzarelli, F. Greco, A. Busilacchi, V. Sollazzo, A. Gigante, Chitosan, hyaluronan and chondroitin sulfate in tissue engineering for cartilage regeneration: A review, Carbohydr. Polym. 89 (2012) 723–739. doi:10.1016/j.carbpol.2012.04.057.

[75] M.K. Yeh, K.M. Cheng, C.S. Hu, Y.C. Huang, J.J. Young, Novel protein-loaded chondroitin sulfate-chitosan nanoparticles: Preparation and characterization, Acta Biomater. 7 (2011) 3804–3812. doi:10.1016/j.actbio.2011.06.026.

[76] K.V. Jardim, G.A. Joanitti, R.B. Azevedo, A.L. Parize, Physico-chemical characterization and cytotoxicity evaluation of curcumin loaded in chitosan/chondroitin sulfate nanoparticles, Mater. Sci. Eng. C. 56 (2015) 294–304. doi:10.1016/j.msec.2015.06.036.

[77] A. Umerska, O.I. Corrigan, L. Tajber, Design of chondroitin sulfate-based polyelectrolyte nanoplexes: Formation of nanocarriers with chitosan and a case study of salmon calcitonin, Carbohydr. Polym. 156 (2017) 276–284. doi:10.1016/j.carbpol.2016.09.035.

[78] F. Furlani, P. Sacco, E. Marsich, I. Donati, S. Paoletti, Highly monodisperse colloidal coacervates based on a bioactive lactose-modified chitosan: From synthesis to characterization, Carbohydr. Polym. 174 (2017) 360–368.

doi:10.1016/j.carbpol.2017.06.097.

[79] A. Gamini, S. Paoletti, F. Zanetti, Chain rigidity of polyuronates:static light scattering of aqueous solutions of hyaluronate and alginate., Laser Ligh (1992) 294–311. https://core.ac.uk/display/53719444 (accessed September 21, 2017).

[80] I. Donati, M. Feresini, A. Travan, E. Marsich, R. Lapasin, S. Paoletti, Polysaccharide-Based Polyanion–Polycation–Polyanion Ternary Systems. A Preliminary Analysis of Interpolyelectrolyte Interactions in Dilute Solutions, Biomacromolecules. 12 (2011) 4044–4056. doi:10.1021/bm201046p.

[81] M. Sartor, Dynamic Light scattering to determine the radiu of small beads in Brownian motion in a solution, (n.d.).

[82] I. Donati, M. Borgogna, E. Turello, A. Casàro, S. Paoletti, Tuning supramolecular structuring at the nanoscale level: Nonstoichiometric soluble complexes in dilute mixed solutions of alginate and lactose-modified chitosan (Chitlac), Biomacromolecules. 8 (2007) 1471–1479. doi:10.1021/bm0610828.

[83] A.B. Kayitmazer, A.F. Koksal, E. Kilic Iyilik, Complex coacervation of hyaluronic acid and chitosan: effects of pH, ionic strength, charge density, chain length and the charge ratio, Soft Matter. 11 (2015) 8605–8612. doi:10.1039/C5SM01829C.

[84] F.A. Oyarzun-Ampuero, J. Brea, M.I. Loza, D. Torres, M.J. Alonso, Chitosan-hyaluronic acid nanoparticles loaded with heparin for the treatment of asthma, Int. J. Pharm. 381 (2009) 122–129. doi:10.1016/j.ijpharm.2009.04.009.

[85] Y. Lapitsky, Ionically crosslinked polyelectrolyte nanocarriers: Recent advances and open problems, Curr. Opin. Colloid Interface Sci. 19 (2014) 122–130. doi:10.1016/j.cocis.2014.03.014.

[86] Q. Gan, T. Wang, C. Cochrane, P. Mccarron, Modulation of surface charge, particle size and morphological properties of chitosan–TPP nanoparticles intended for gene delivery, Colloids Surfaces B Biointerfaces. 44 (2005) 65–73. doi:10.1016/j.colsurfb.2005.06.001.

[87] B. Hu, C. Pan, Y. Sun, Z. Hou, H. Ye, X. Zeng, Optimization of Fabrication Parameters To Produce Chitosan-Tripolyphosphate Nanoparticles for Delivery of Tea Catechins, J. Agric. Food Chem. (2008). doi:10.1021/jf801111c.

[88] H. Zhang, M. Oh, C. Allen, E. Kumacheva, Monodisperse Chitosan Nanoparticles for Mucosal Drug Delivery, Biomacromolecules. (2004). doi:10.1021/bm0496211.

[89] H. Li, X. Zhao, Y. Ma, G. Zhai, L. Li, H. Lou, Enhancement of gastrointestinal absorption of quercetin by solid lipid nanoparticles, J. Control. Release. 133 (2009) 238–244. doi:10.1016/j.jconrel.2008.10.002.

[90] R. Menegazzi, S. Busetto, P. Dri, R. Cramer, P. Patriarca, Chloride ion efflux regulates adherence, spreading, and respiratory burst of neutrophils stimulated by tumor necrosis factor-α (TNF) on biologic surfaces, J. Cell Biol. 135 (1996) 511–522. doi:10.1083/jcb.135.2.511.

[91] P. Dri, R. Cramer, P. Spessotto, M. Romano, P. Patriarca, EOSINOPHIL ACTIVATION ON BIOLOGIC SURFACES ’ I s Differentially Production of 0 ; in Response to Physiologic Soluble Stimuli Modulated by Extracellular Matrix Components and Endothelial Cells, (1991).

[92] D. Priftis, K. Megley, N. Laugel, M. Tirrell, Complex coacervation of poly(ethylene-imine)/polypeptide aqueous solutions: Thermodynamic and rheological characterization, J. Colloid Interface Sci. 398 (2013) 39–50. doi:10.1016/j.jcis.2013.01.055.

[93] V.A. Izumrudov, I.F. Volkova, E.S. Grigoryan, M.Y. Gorshkova, Water-soluble

nonstoichiometric polyelectrolyte complexes of modified chitosan, Polym. Sci. Ser. A. 53 (2011) 281–288. doi:10.1134/S0965545X11040043.

[94] Y. Huang, Y. Lapitsky, Salt-assisted mechanistic analysis of chitosan/tripolyphosphate micro- and nanogel formation., Biomacromolecules. 13 (2012) 3868–76. doi:10.1021/bm3014236.

[95] A. Rampino, M. Borgogna, P. Blasi, B. Bellich, A. Cesàro, Chitosan nanoparticles: Preparation, size evolution and stability, Int. J. Pharm. 455 (2013) 219–228. doi:10.1016/j.ijpharm.2013.07.034.

[96] D.W. Edlow, H. Sheldon, The pH of inflammed exudates, Exp. Biol. Med. (1971) 1328–1332.

[97] R.H. Boots, G.E. Cullen, the Hydrogen Ion Concentration of Joint Exudates in Rheumatic Fever and Other Forms of Arthritis., J. Exp. Med. 36 (1922) 405–14. doi:10.1084/jem.36.4.405.

[98] J.L. Wike-Hooley, J. Haveman, H.S. Reinhold, The relevance of tumour pH to the treatment of malignant disease, Radiother. Oncol. 2 (1984) 343–366. doi:10.1007/978-3-658-09837-7.

[99] N.M. Zaki, A. Nasti, N. Tirelli, Nanocarriers for cytoplasmic delivery: cellular uptake and intracellular fate of chitosan and hyaluronic acid-coated chitosan nanoparticles in a phagocytic cell model., Macromol. Biosci. 11 (2011) 1747–60. doi:10.1002/mabi.201100156.

[100] C. Nathan, S. Srimal, C. Farber, E. Sanchez, L. Kabbash, A. Asch, J. Gailit, S.D. Wright, Cytokine-induced respiratory burst of human neutrophils: Dependence on extracellular matrix proteins and CD11/CD18 integrins, J. Cell Biol. 109 (1989) 1341–1349. doi:10.1083/jcb.109.3.1341.

[101] L.J. Lin, J.M. Grimme, J. Sun, S. Lu, L. Gai, D.M. Cropek, Y. Wang, The antagonistic roles of PDGF and integrin αvβ3 in regulating ROS production at focal adhesions, Biomaterials. 34 (2013) 3807–3815. doi:10.1038/jid.2014.371.

[102] E. Bahar, J.Y. Kim, H. Yoon, Quercetin attenuates manganese-induced neuroinflammation by alleviating oxidative stress through regulation of apoptosis, iNoS/NF-κB and HO-1/Nrf2 pathways, Int. J. Mol. Sci. 18 (2017). doi:10.3390/ijms18091989.

[103] P.C.A. and C.Z. Andrew R. Thoreson, Ryo Hiwatari, Kai-Nan An, The Effect of 1-Ethyl-3-(3-Dimethylaminopropyl) Carbodiimide Suture Coating on Tendon Repair Strength and Cell Viability in A Canine Model, J Hand Surg Am. 40 (2015) 1986–1991. doi:10.1038/nrg3575.Systems.

[104] P. Rakesh, K. Vipin, K. Kanchan, Alginate Beads Prepared by Ionotropic Gelation Technique: Formulation Design, Res. J. Chem. Sci. _____ ISSN 2231-606X. 5 (2015) 45. www.isca.me.

[105] T. Kokubo, S. Ito, Z.T. Huang, T. Hayashi, S. Sakka, T. Kitsugi, T. Yamamuro, Ca, P-rich layer formed on high-strength bioactive glass-ceramic A-W, J. Biomed. Mater. Res. 24 (1990) 331–343. doi:10.1002/jbm.820240306.

[106] M. Wong, Alginates in tissue engineering., Methods Mol. Biol. 238 (2004) 77–86. doi:10.1385/1-59259-428-X:77.

[107] C. Little, W. Kulyk, X. Chen, The Effect of Chondroitin Sulphate and Hyaluronic Acid on Chondrocytes Cultured within a Fibrin-Alginate Hydrogel, J. Funct. Biomater. 5 (2014) 197–210. doi:10.3390/jfb5030197.

[108] E. Marsich, F. Bellomo, G. Turco, A. Travan, I. Donati, S. Paoletti, Nano-composite

scaffolds for bone tissue engineering containing silver nanoparticles: Preparation, characterization and biological properties, J. Mater. Sci. Mater. Med. 24 (2013) 1799–1807. doi:10.1007/s10856-013-4923-4.

[109] K.Y.L. and D.J. Mooney, Alginate: properties and biomedical applications, Prog Polym Sci. 37 (20012) 106–126. doi:10.1016/j.progpolymsci.2011.06.003.Alginate.

[110] B.F. Gibbs, S. Kermasha, Encapsulation in the food industry - a review.pdf, (1999) 213–224.

[111] P. Agulhon, V. Markova, M. Robitzer, F. Quignard, T. Mineva, Structure of alginate gels: Interaction of diuronate units with divalent cations from density functional calculations, Biomacromolecules. 13 (2012) 1899–1907. doi:10.1021/bm300420z.

[112] J.T. Oliveira, L. Martins, R. Picciochi, P.B. Malafaya, R.A. Sousa, N.M. Neves, J.F. Mano, R.L. Reis, Gellan gum: A new biomaterial for cartilage tissue engineering applications, J. Biomed. Mater. Res. - Part A. 93 (2010) 852–863. doi:10.1002/jbm.a.32574.

[113] A. Franck, Understanding rheology of structured fluids, B. TA Instruments. (2004) 1–11. http://scholar.google.com/scholar?hl=en&btnG=Search&q=intitle:Understanding+Rheology+of+Structured+Fluids#2%5Cnhttp://scholar.google.com/scholar?hl=en&btnG=Search&q=intitle:Understanding+rheology+of+structured+fluids%232.

[114] O. Chaudhuri, L. Gu, D. Klumpers, M. Darnell, S.A. Bencherif, J.C. Weaver, N. Huebsch, H.P. Lee, E. Lippens, G.N. Duda, D.J. Mooney, Hydrogels with tunable stress relaxation regulate stem cell fate and activity, Nat. Mater. 15 (2016) 326–334. doi:10.1038/nmat4489.

[115] J.R. Mitchell, J.M.V. Blanshard, Rheological properties of alginates, J. Texture Stud. 7 (1976) 219–234. doi:10.1246/nikkashi.1994.108.

[116] R.M. Ottenbrite, Biomedical Applications of Hydrogels Handbook, Springer. (2010). doi:10.1007/978-1-4419-5919-5.

[117] L. Li, G. Zhou, Y. Wang, G. Yang, S. Ding, S. Zhou, Controlled dual delivery of BMP-2 and dexamethasone by nanoparticle-embedded electrospun nanofibers for the efficient repair of critical-sized rat calvarial defect, Biomaterials. 37 (2015) 218–229. doi:10.1016/j.biomaterials.2014.10.015.